Molecular Pharmacology Fast Forward. Published on October 3, 2019 as DOI: 10.1124/mol.119.116657
This article has not been copyedited and formatted. The final version may differ from this version.

1. Title page

Conformational Changes in the 5-HT_{3A} Receptor Extracellular Domain Measured by Voltage Clamp Fluorometry

Lachlan Munro[1], Lucy Kate Ladefoged[2], Vithushan Padmanathan[1], Signe Andersen[1], Birgit Schiøtt[2, 3], Anders S. Kristensen[1]

[1]Department of Drug Design and Pharmacology, University of Copenhagen, Universitetsparken 2, DK-2100 Copenhagen, Denmark

[2] Department of Chemistry, Aarhus University, Langelandsgade 140, DK-8000 Aarhus, Denmark

[3]Interdisciplinary Nanoscience Center (iNANO), Aarhus University, Langelandsgade 140, DK-8000 Aarhus, Denmark

Molecular Pharmacology Fast Forward. Published on October 3, 2019 as DOI: 10.1124/mol.119.116657
This article has not been copyedited and formatted. The final version may differ from this version.

2. Running title page

Running title:

Ligand Specific Conformational Changes at the 5-HT_3 Receptor

Corresponding author information:

Anders S. Kristensen, Department of Drug Design and Pharmacology, University of Copenhagen, Universitetsparken 2, DK-2100 Copenhagen, Denmark. E-mail: ask@sund.ku.dk. Tel.: +45 35 30 65 05

Abbreviations used:

5-HT: 5-hydroxytryptamine; 5-HTBP: 5-HT binding protein; ACh: Acetylcholine; AChBP: Acetylcholine binding protein; CNS: central nervous system; Cryo-EM: Cryo-electron microscopy; DMEM: Dulbecco's modified Eagle's medium; ECD: extracellular domain; FPS: FRET positioning and screening; GABA: γ-aminobutyric acid; h5-HT_{3A}: human 5-HT_{3A}; m5-HT_{3A}: mouse 5-HT_{3A}; mCPBG: 1-(m-chlorophenyl)-biguanide, MD: molecular dynamics; MTS-TAMRA: 2-((5(6)-tetramethylrhodamine)carboxylamino)ethyl methanethiosulfonate; pLGIC: pentameric ligand-gated ion channel; PMT: photomultiplier tube; TEVC: two-electrode voltage clamp; TMD: transmembrane domain; VCF: voltage-clamp fluorometry.

Molecular Pharmacology Fast Forward. Published on October 3, 2019 as DOI: 10.1124/mol.119.116657
This article has not been copyedited and formatted. The final version may differ from this version.

3. Abstract

The 5-HT_3 receptor is a member of the Cys-loop receptor super family of ligand-gated ion channel in the nervous system and is a clinical target in a range of diseases. The 5-HT_3 receptor mediates fast serotonergic neurotransmission by undergoing a series of conformational changes initiated by ligand-binging that lead to the rapid opening of an intrinsic cation-selective channel. However, despite the availability of high-resolution structures of a mouse 5-HT_3 receptor, many important aspects of the mechanistic basis of 5-HT_3 receptor function and modulation by drugs remain poorly understood. In particular, there is little direct evidence for the specific conformational changes predicted to occur during ligand-gated channel activation and desensitization.

In the present study, we used voltage-clamp fluorometry (VCF) to measure conformational changes in regions surrounding the orthosteric binding site of the human 5-HT_{3A} (h5-HT_{3A}) receptor during binding of 5-HT and different classes of 5-HT_3 receptor ligands. VCF utilizes parallel measurements of receptor currents with photon emission from fluorescent reporter groups covalently attached to specific positions in the receptor structure. Reporter groups that are highly sensitive to the local molecular environment can in real-time report conformational changes as changes in fluorescence that can be correlated with changes in receptor currents reporting the functional states of the channel. Within the loop C-, D-, and E-regions that surround the orthosteric binding site in the h5-HT_{3A} receptor, we identify positions that are amenable to tagging with an environmentally sensitive reporter group that reports robust fluorescence changes upon 5-HT binding and receptor activation. We use these reporter positions to characterize the effect of ligand binding on the local structure of the orthosteric binding site by agonists, competitive antagonists, and allosterically acting channel activators. We observed that loop C appears to show distinct fluorescence changes for ligands of the same class, while loop D reports similar fluorescence

Molecular Pharmacology Fast Forward. Published on October 3, 2019 as DOI: 10.1124/mol.119.116657
This article has not been copyedited and formatted. The final version may differ from this version.

changes for all ligands binding at the orthosteric site. In contrast, the loop E reporter position shows distinct changes for agonists, antagonists, and allosteric compounds, suggesting the conformational changes in this region are specific to ligand function. Interpretation of these results within the framework of current models of 5-HT_3 and Cys-loop mechanisms are used to expand the understanding of how ligand binding in Cys-loop receptors relates to channel gating.

Molecular Pharmacology Fast Forward. Published on October 3, 2019 as DOI: 10.1124/mol.119.116657
This article has not been copyedited and formatted. The final version may differ from this version.

4. Significance statement

The $5HT_3$ receptor is an important ligand-gated ion channel and drug target in the central and peripheral nervous system. Determining how ligand binding induced conformational changes in the receptor is central for understanding the structural mechanisms underlying $5HT_3$ receptor function. Here, we employ voltage-gated fluorometry to characterize conformational changes in the extracellular domain of the human $5HT_3$ receptor to identify intra-receptor motions during binding of a range of 5HT3 receptor agonists and antagonists.

Molecular Pharmacology Fast Forward. Published on October 3, 2019 as DOI: 10.1124/mol.119.116657
This article has not been copyedited and formatted. The final version may differ from this version.

5. Introduction

5-HT_3 receptors in the central nervous system transduce fast synaptic transmission and are considered therapeutic targets for the treatment of chemotherapy-induced nausea and vomiting and psychiatric conditions such as schizophrenia and depression (Thompson & Lummis, 2007; Walstab et al., 2010). Furthermore, 5-HT_3 receptors in the enteric nervous system regulate gut motility and are well-established targets for the treatment of irritable bowel syndrome (Lummis, 2012). 5-HT_3 receptors belong to the pentameric ligand-gated ion channel (pLGIC) superfamily, also known as Cys-loop receptors (Nemecz et al., 2016). pLGICs have as structural hallmark five subunits forming a central ion-permeable pore in the transmembrane domain (TMD; Fig. 1A) with orthosteric ligand binding sites located at subunit interfaces in the extracellular domain (ECD; Fig. 1A). pLGICs are thought to share a common structural mechanism for how agonist binding in the ECD couples to channel activation and desensitization in the TMD (Grosman et al., 2000; Barnes et al., 2009; Corringer et al., 2010; Lummis, 2012; Nys et al., 2013; Keramidas and Lynch, 2013; Nemecz et al., 2016).

Detailed structural information is available for the 5-HT_3 receptor in the form of X-ray crystal and cryo-electron microscopy (cryo-EM) structures of the mouse 5-HT_{3A} (m5-HT_{3A}) receptor (Hassaine et al., 2014; Basak, Gicheru, Rao, et al., 2018; Basak, Gicheru, Samanta, et al., 2018; Polovinkin et al., 2018). Also, the acetylcholine binding protein (AChBP), which is a soluble pentameric eukaryotic protein homologous to the ECD of Cys-loop receptors (Brejc et al., 2001; Sixma & Smit, 2003) has been engineered to mimic the 5-HT_3 receptor ligand binding profile (Kesters et al., 2012). Crystal structures of this construct (5-HT binding protein, denoted 5-HTBP) in complex with 5-HT, granisetron (Kesters et al., 2012), palonosetron (Price et al., 2016) and varenicline (Price et al., 2015) provide atomic-level insight to potential ligand binding modes and local conformations of the ECD in the 5HT_3 receptor. However, the binding mode of 5-HT, as well

Molecular Pharmacology Fast Forward. Published on October 3, 2019 as DOI: 10.1124/mol.119.116657
This article has not been copyedited and formatted. The final version may differ from this version.

as the local conformation of the binding sites observed in the 5-HTBP structure (Kesters et al., 2012), is different to the binding modes of 5-HT observed in recently reported cryo-EM structures of the mouse 5-HT_3 (m5-HT_3) receptor (Basak et al., 2018a; Polovinkin et al., 2018). Thus, there are still gaps in the understanding of how ligand binding in the orthosteric site can either induce or prevent the opening of the relatively distal ion channel; partly due to a lack of data describing specific intra-receptor motions during ligand binding.

Voltage-clamp fluorometry (VCF) is a technique that uses site-specific labeling of proteins with an environmentally sensitive fluorophore coupled with two-electrode voltage-clamp electrophysiology (TEVC) (Mannuzzu et al., 1996). VCF allows simultaneous real-time measurement of both the functional state of an ion channel and conformational changes around specific regions, which are reported as changes in fluorescence intensity (ΔF) (Talwar & Lynch, 2015). Previously, VCF has been used to investigate conformational changes in the ECD of other Cys-loop receptors such as the glycine receptor (Pless & Lynch, 2009a; Lynagh & Lynch, 2012; Soh et al., 2017), the $GABA_A$ receptor (Chang & Weiss, 2002; Khatri et al., 2009; Muroi et al., 2009; Akk et al., 2011; Eaton et al., 2014), the nicotinic acetylcholine receptor (Dahan et al., 2004) and very recently, used to track conformational changes in the ion pore region of the m5-HT_3 receptor associated with channel gating (Polovinkin et al., 2018).

In the present study, we utilize VCF to monitor conformational changes in the ECD around the orthosteric site of the human 5-HT_{3A} (h5-HT_{3A}) receptor induced by binding of agonists, antagonists, and allosteric modulators. At the 5-HT_3 subunit interfaces, the orthosteric binding sites are formed by six segments (designated loop A to F; Fig 1). Specifically, we identify reporter positions in loop C, E and F where residues are amenable to replacement with cysteine (Cys) and labeling with the fluorophore 2-([5(6)-tetramethyl-rhodamine] carboxylamino) ethyl methanethiosulfonate (MTS-TAMRA) and can report ligand-induced structural rearrangements as

Molecular Pharmacology Fast Forward. Published on October 3, 2019 as DOI: 10.1124/mol.119.116657
This article has not been copyedited and formatted. The final version may differ from this version.

changes in TAMRA fluorescence. In agreement with VCF studies of other Cys-loop receptors, our findings indicate that the loop E reporter position display distinct ΔF for agonists and antagonists. A loop D reporter position was found to report similar ΔF in response to all orthosteric binding ligands, regardless of function. We also observe that functionally and structurally similar antagonists can induce distinct ΔF at a reporter position in loop C.

Molecular Pharmacology Fast Forward. Published on October 3, 2019 as DOI: 10.1124/mol.119.116657
This article has not been copyedited and formatted. The final version may differ from this version.

6. Materials and Methods

Materials – Chemicals were from Sigma (St. Louis, MO) except when otherwise stated. DNA modifying enzymes were from New England Biolabs (Ipswich, MA). Granisetron, ondansetron, tropisetron, mirtazapine, thymol, and carvacrol were from Tokyo Chemical Industry (Zwijndrecht, Belgium). *m*-chlorophenyl biguanide (mCPBG) was from Tocris Bioscience (Bristol, UK). 2-([5(6)-Tetramethyl-rhodamine] carboxylamino) ethyl methanethiosulfonate (MTS-TAMRA) was from Biotium (Hayward, CA).

Molecular Biology – cDNA encoding h5-HT_{3A} was kindly provided by Beate Niesler (Dept. of Human Molecular Genetics, University of Heidelberg, Heidelberg). For expression in *Xenopus laevis* oocytes, the h5-HT_{3A} coding region was subcloned into the pXOON expression vector as described previously (Ladefoged et al., 2018). Cysteine (Cys) mutations were introduced using the QuickChange site-directed mutagenesis kit from Stratagene (La Jolla, CA). Successful mutagenesis was confirmed by sequencing of the entire coding region (GATC Biotech, Constance, Germany). mRNA was generated using the AmpliCap T7 High Yield Message Maker Kit (CellScript, Madison, WI) according to the manufacturer's instructions.

Xenopus Laevis Oocyte Expression – Defoliated stage V to VI oocytes from *Xenopus laevis* were prepared as described previously (Poulsen et al., 2014) and injected with 15 ng mRNA. The care and use of *Xenopus laevis* were in strict adherence to a protocol (license 2014−15−0201−00031) approved by the Danish Veterinary and Food Administration. Injected oocytes were incubated at 18 °C for 3 to 10 days in Standard Barth's Medium containing (in mM) 88 NaCl, 1 KCl, 0.41 $CaCl_2$, 2.4 $NaHCO_3$, 0.33 $Ca(NO_3)_2$, 0.82 $MgSO_4$, 5 Tris (pH 7.4) supplemented with 50 μg/ml gentamycin. Healthy oocytes that showed robust expression were stored at 4 °C for up to 5 additional days.

Molecular Pharmacology Fast Forward. Published on October 3, 2019 as DOI: 10.1124/mol.119.116657
This article has not been copyedited and formatted. The final version may differ from this version.

Labeling of oocytes – Oocytes were transferred to frog Ringer's solution (115 mM NaCl, 2 mM KCl, 5 mM HEPES, 1.8 mM BaCl, pH 7.6) containing 20 μM MTS-TAMRA and left for 30 seconds in the dark at room temperature. Oocytes were then rinsed three times in frog Ringer's solution. Labeled oocytes were kept in Ringer's solution in the dark for up to two hours before recording.

Electrophysiology and Voltage Clamp Fluorometry – VCF recordings were performed essentially as described previously (Soderhielm et al., 2015). A glass bottom perfusion chamber was mounted on an inverted epifluorescence microscope (Diaphot 300; Nikon, Japan) equipped with a 20x air objective and a G-1B filter set (Chroma 11002v2, excitation filter 541-551 nm, dichroic mirror > 565 nm, emission > 590 nm). Excitation was achieved using an LED lamp with a nominal wavelength of 530 nm (M530L3; ThorLabs, Newton, NJ). Fluorescence intensity was measured with a D104 photomultiplier tube (PMT) system (Photon Technologies International). PMT voltage was adjusted daily between 450 and 700 volts such that baseline converted fluorescence output on labeled oocytes was between 0.5 and 5 volts. Membrane current was measured under two-electrode voltage clamp (TEVC). Oocytes were voltage-clamped at -20 mV and continuously perfused with frog Ringer's. All ligands were dissolved in frogs Ringer's solution and applied using an automated programmable perfusion system (Bioscience Tools, San Diego, CA). Current, voltage and fluorescence signals were digitized at 200 Hz (DigiData 1332, Molecular Devices, Sunnyvale, CA) and recorded using a PC running Clampex 10 software (Molecular Devices, Sunnyvale, CA). For fluorescence antagonist dose-response curves, each concentration was applied for two minutes to allow stable fluorescence levels. The excitation LED was pulsed for 200 ms every second to limit the fluorophore photodestruction during the extended recording time. For fast-solution switching electrophysiology experiments to determine rates of activation, deactivation, and desensitization, we utilized a vertical flow chamber with a chamber volume of 200 μL (Joshi at al., 2004). With a

Molecular Pharmacology Fast Forward. Published on October 3, 2019 as DOI: 10.1124/mol.119.116657
This article has not been copyedited and formatted. The final version may differ from this version.

constant flow rate of 20 mL/min, this chamber design results in complete solution exchange within ~500 ms as measured by recordings open-tip pipette potential when the pipette is positioned just above the oocyte in response to exchange of high and low molarity.

Molecular modeling – A previously generated homology model of h5-HT_{3A} (Ladefoged et al., 2018) was used as a starting point for the creation of models of h5-HT_{3A} receptor Cys-mutants with TAMRA conjugated. Specifically, for each reporter position (Tyr89, Met223, and Gln146), the wild-type residue was mutated to a Cys using the mutate tool within Maestro 10.1 (Schrödinger Suite, 2015). The TAMRA molecule including the linker was built in Maestro 10.1 and minimized using a conjugate-gradient algorithm in MacroModel 10.7. The protonation state of the TAMRA molecule was assessed using Epik 3.1 (Shelley et al., 2007; Greenwood et al., 2010) and was modeled in a zwitterionic state. TAMRA structural conformation was optimized using MacroModel 10.7 and a 1000-step mixed torsional/low-mode sampling conformational search algorithm in which a 2500-step minimization followed each step with all other settings at default. Insertion of TAMRA and MTS linker at Cys residues was performed by structurally aligning S-C_β-C_α atoms from the Cys side chain to S-CH_2-CH_3 heavy atoms from the linker. Duplicate atoms were deleted, and the atomic bond between the linker and the reporter position side chain was drawn manually in Maestro 10.1. The QuickTorsion tool available in Maestro was used to move linker and TAMRA molecule out of direct steric clashes with the protein. The resulting TAMRA-linked h5-HT_{3A} structure was further processed using the Protein Preparation Wizard (Sastry et al., 2013). Specifically, the conjugated TAMRA including linker and protein residues within 5 Å were subjected to energy minimization using a conjugate gradient algorithm and a conformational search using the substructure option in MacroModel 10.7, while residues in the 5 to 10 Å distance range were restrained by a force constant of 200 kJ/(mol $Å^2$). All remaining atoms were ignored during the calculation. Calculation of accessible volume for TAMRA at each reporter position was performed

Molecular Pharmacology Fast Forward. Published on October 3, 2019 as DOI: 10.1124/mol.119.116657
This article has not been copyedited and formatted. The final version may differ from this version.

using the FRET positioning and screening (FPS) software (Kalinin et al., 2012). This software estimates the volume accessible to the MTS-linked TAMRA molecule at each reporter position using a geometric search algorithm. The fluorophore is approximated by a sphere, and the linker is simply treated as a distance. The search algorithm determines all possible orientations and positions the fluorophore can reach based on the applied linker that does not clash sterically with the protein. Before each calculation, the side chain of the reporter positions in subunit A (Met223 from the principal face) or E (Tyr89 and Gln146 from the complementary face) was removed to prevent the original residue from causing steric clashes with the fluorophore probe. Three parameters were used to describe MTS-TAMRA during calculations: linker length (16 Å), linker width (3 Å), and dye radii (x, y, z is 7, 5, and 3 Å, respectively). The dimensions were estimated based on a computational model of MTS-TAMRA in a stretched conformation, and the linker length is the distance from the distal end of the linker to the geometric center of TAMRA.

Data and Statistical Analysis –Data and statistical analyses were performed using pClamp 10 (Molecular Devices) or Prism 6.0 (GraphPad Inc., San Diego, CA) software. Calculation of ΔF was performed using the equation:

$$\Delta F = \frac{F_{Peak} - F_{Baseline}}{F_{Baseline}}$$

Where F_{peak} is the peak fluorescence observed following application of ligand and $F_{baseline}$ is the fluorescence immediately before ligand application. For EC_{50} determination, current or fluorescence responses were normalized to the maximal ΔF or current response in each oocyte and pooled. The composite concentration-response data analyzed by iterative curve fitting using the equation:

$$\text{Response} = \frac{1}{(1 + 10^{(\text{LogY} - \text{X}) \times \text{nH}})}$$

Molecular Pharmacology Fast Forward. Published on October 3, 2019 as DOI: 10.1124/mol.119.116657
This article has not been copyedited and formatted. The final version may differ from this version.

where Response is the ΔF or current response measured at a given concentration normalized to the maximum response, Y is the concentration of ligand that produces a half-maximal response (EC_{50}), X is the logarithm of the concentration of the ligand, and nH is the Hill slope. Unless otherwise noted, data are reported as either mean ± SEM or mean with 95 % confidence intervals. Statistical analysis of pairwise or multiple comparisons was performed using ANOVA or Student's t-test as appropriate. A probability value (p) < 0.05 was considered statistically significant.

Molecular Pharmacology Fast Forward. Published on October 3, 2019 as DOI: 10.1124/mol.119.116657
This article has not been copyedited and formatted. The final version may differ from this version.

7. Results

Identification of VCF reporter positions in h5-HT$_{3A}$ – To investigate ligand-induced structural changes in 5-HT$_3$ receptors, we first searched for residues in homomeric h5-HT$_{3A}$ receptors that were amenable to substitution with Cys and thiol-mediated fluorophore conjugation. However, a prerequisite of this type of site-specific fluorophore labeling is the absence of endogenous Cys residues that are extracellularly accessible and thiol-reactive. Structures of the m5-HT$_{3A}$ receptor (Hassaine et al., 2014; Basak et al., 2018a; Polovinkin et al., 2018; Basak et al., 2018b; Basak et al., 2019) show that the only Cys residues in the ECD are Cys157 and Cys171 in the eponymous Cys-loop. Cys157 and Cys171 form a disulfide bond and thus should not be reactive towards MTS-TAMRA (Fig. 1B). Also, previous experiments utilizing thiol-reactive fluorophores on other Cys-loop receptors have found this pair of conserved Cys residues to be inaccessible to labeling (Dahan et al., 2004; Pless & Lynch, 2009a; Eaton et al., 2014). However, to verify that potential labeling of Cys157 and Cys171 did not produce background signals, we initially subjected oocytes expressing wild-type (WT) h5-HT$_{3A}$ receptors to MTS-TAMRA labeling and measured fluorescence during application of different ligands (*Materials and methods*). Following treatment with MTS-TAMRA, application of 100 μM 5-HT to WT h5-HT$_{3A}$ expressing oocytes showed no or less than 1 % ΔF and was in general indistinguishable from fluorescence recordings at MTS-TAMRA treated uninjected oocytes (Fig. 1C and D). On this basis, we concluded that the WT h5-HT$_{3A}$ receptor formed a suitable background for the introduction of Cys residues for VCF.

We next sought to identify residues in the h5-HT$_{3A}$ receptor subunit useful as VCF reporter positions following substitution with Cys and MTS-TAMRA labeling. Criteria for a residue position to be a useful reporter include that *i*) the position must allow the side chain of the introduced Cys residue to be accessible to an extracellularly applied thiol-reactive fluorophore, *ii*) Cys-mutation does not interfere excessively with subunit assembly and normal receptor function,

Molecular Pharmacology Fast Forward. Published on October 3, 2019 as DOI: 10.1124/mol.119.116657
This article has not been copyedited and formatted. The final version may differ from this version.

and *iii*) be capable of reporting ΔF in response to conformational changes at the labeled position. Extensive cysteine scans often yield only a small number of useful VCF reporter positions (Zhang et al., 2009; Talwar & Lynch, 2015). To improve the rate of identifying successful reporter residues, we used previously performed VCF work on other Cys-loop receptors as a guide to residue selection (Table 1 and Supplementary Fig. S1). On this basis, seven h5-HT_{3A} residues around the orthosteric binding site were selected for mutation to Cys (Fig. 1B and Table 1). Also, we sought to identify reporter positions for movements occurring outside the orthosteric binding site; potentially leading toward channel activation. The pre-M1 region is known to couple conformational changes between the orthosteric binding site and the channel and to rearrange before opening of the channel gate (Castaldo et al., 2004; Purohit et al., 2013), which via structures of the $5HT_{3A}$ receptor in various functional states have been identified to be formed by residues located roughly in the middle of transmembrane helix M2 that lines the pore (Polovinkin et al., 2018; Basak, Gicheru, Rao, et al., 2018). We, therefore, performed scanning Cys mutagenesis along the pre-M1 region; introducing Cys at a further seven positions (Fig. 1B and Table 1).

We expressed Cys-mutant receptors individually in *Xenopus* oocytes and, following labeling with MTS-TAMRA, evaluated for current and ΔF responses to the application of 100 μM 5-HT (*Materials and methods*) (Fig. 1B). As summarized in Fig. 1D, all tested mutants showed inward currents in response to 5-HT with amplitudes that were within the range observed for the WT receptor. Four mutants (Y89C, M223C, F221C, and Q146C) were found to report robust ΔF in response to 100 μM 5-HT (Fig. 1C and D). These mutants all showed increased fluorescence in response to 5-HT with mean ΔF values of 30 ± 2 % (Y89C), 11 ± 1 % (Q146C), 4.6 ± 0.7 % (F221C), and 14 ± 1 % (M223C) (Fig. 1B and C). The remaining mutants did not report detectable ΔF in response to 100 μM 5-HT or produced ΔF that were less than 2-fold of background fluorescence and were not investigated further. A caveat of VCF when using reporter positions near

Molecular Pharmacology Fast Forward. Published on October 3, 2019 as DOI: 10.1124/mol.119.116657
This article has not been copyedited and formatted. The final version may differ from this version.

ligand binding sites is that fluorescence changes may theoretically indicate a change in microenvironment due to proximity to the ligand and not a conformational change in the protein. We determined the effect of 5-HT on TAMRA fluorescence in solution (*Materials and Methods)*. 5-HT caused a concentration-dependent decrease of TAMRA fluorescence intensity with no change in the peak emission wavelength (*Supplementary Fig. S2).* Thus, if bound 5-HT exerts a direct effect on the fluorescence of receptor-conjugated TAMRA, this would be reported as a decrease in fluorescence or negative ΔF. As the ΔF observed during VCF at all positions were positive, we concluded that the observed changes in fluorescence are not caused by direct fluorophore-ligand interaction. Consequently, we assume that the ΔF observed in response to 5-HT indicates local or global conformational changes of the protein.

Characterization of reporter position Cys mutants – To evaluate if Cys-mutation and TAMRA-labeling change basal ligand-gated ion channel properties of the potential reporter Cys-mutants, we performed electrophysiological characterization of 5-HT response kinetics and EC_{50} (Fig. 2 and Table 2). First, we determined EC_{50} for 5-HT at WT and the Y89C, M223C, Q146C, and F221C mutant receptors with and without MTS-TAMRA treatment (Fig. 2A). With and without labeling, the Y89C and Q146C mutant showed EC_{50} values that were within close range of the EC_{50} for the WT receptor (Table 2). In contrast, there was a profound decrease in 5-HT potency for the F221C mutant with a 47-fold increase in EC_{50}, which upon TAMRA labeling further increased to more than 150-fold relative to WT (Table 2). The M223C mutant displayed a 3-fold increase in EC_{50} relative to WT and increased further to 12-fold upon TAMRA labeling (Table 2). The Phe221 and Met223 positions are located very near each other on loop C and therefore likely report the same conformational changes. The VCF screening results suggested that the M223C mutant, in general, displayed stronger fluorescence signals compared to F221C (Fig. 1C). Therefore, due to the

Molecular Pharmacology Fast Forward. Published on October 3, 2019 as DOI: 10.1124/mol.119.116657
This article has not been copyedited and formatted. The final version may differ from this version.

profound effect of Cys-mutation and TAMRA labeling on the EC_{50} for 5-HT for the F221C mutant and its generally weaker fluorescence signals, we abandoned further work with the F221C mutant.

To further characterize the potential effects of Cys-mutations and TAMRA-labeling on receptor function, we performed fast ligand-application experiments to determine the 5-HT response kinetics. Specifically, using a vertical oocyte perfusion chamber that allows solution exchange rates in the 100 to 500 ms range (Joshi et al., 2004) (*Methods and materials*), we characterized the rate of activation, desensitization and deactivation of currents evoked by application of saturating concentration (1 mM) of 5-HT to oocytes expressing WT and Y89C, Q146C, and M223C mutant receptors (Fig. 2B). The obtained time constants for activation (τ_{act}), deactivation (τ_{deact}), and desensitization (τ_{desens}) were in good agreement with previously reported characteristics of 5-HT_{3A} receptor currents recorded from oocytes (Jackson & Yakel, 1995; Yakel, 1996; Davies et al., 1999; Dubin et al., 1999; Joshi et al., 2004). Furthermore, the results showed that the Cys-mutations and TAMRA labeling has no or little effect on receptor kinetics; except for a modest 3-fold decrease of the activation rate for the Q146C mutant upon TAMRA labeling (Fig. 2C). In summary, the Y89C, Q146C, and M223C mutants overall retain receptor properties similar to WT, and we, therefore, selected all three mutants for further VCF experimentation.

Modeling TAMRA at the three reporter positions - To investigate how the Cys-conjugated TAMRA molecule at the 89, 146, and 223 positions relate to the orthosteric binding site, we generated models of the h5-HT_{3A} receptor in the inactive conformation with the fluorophore attached at the three reporter sites (Fig. 3A) and calculated the volume accessible to the fluorophore at each position (*Materials and Methods*). The models show that the fluorophore at the 89 and 146 positions in loop D and E, respectively, are well-accommodated by the protein and can move freely around the complementary face of the binding site (Fig. 3B and C). The accessible volume at these two reporter positions overlap directly in front of loop D and E moreover, are also close to loop C.

Molecular Pharmacology Fast Forward. Published on October 3, 2019 as DOI: 10.1124/mol.119.116657
This article has not been copyedited and formatted. The final version may differ from this version.

However, only at position 89, TAMRA can reach loop B from the principal face and only at position 146, TAMRA can reach loop F and G (Fig. 3B and C). Due to the flexible nature of the linker and loop C itself, TAMRA at position 223 can sample a large portion of both the principal and complementary subunit when loop C is in an extended conformation such as observed in structures thought to represent the receptor in an inactive state (Fig. 3D). In contrast, when loop C is closed in on the binding site as is suggested to occur during activation, movement of the fluorophore is likely dynamically restricted by loop C as the Cys side chain at position 223 is facing the binding site. Importantly, based on the accessible volume calculations, the TAMRA molecule at position 223 is able to occupy the orthosteric binding site and possibly compete with the tested ligands, which may explain the increase in agonist EC_{50} observed for the M223C mutant following TAMRA labeling (Fig. 2A). In summary, the results from the TAMRA modeling indicate that the TAMRA conjugated at position 89, 146, and 223 collectively cover the space surrounding the orthosteric binding site.

Fluorometric characterization of ligand-induced conformational changes – At present, there is a complete lack of direct experimental evidence of the conformational changes in the ECD that are induced by different classes of 5-HT_3 ligands and their correlation to ligand functional effects. We, therefore, measured ΔF in response to a range of structurally and functionally diverse 5-HT_3 ligands (Fig. 4A) at the Y89C, M223C, and Q146C mutants. These ligands included the orthosteric ligands acting as agonists (5-HT and mCPBG) and competitive antagonists (granisetron, ondansetron, tropisetron, and encenicline) as well as the positive allosteric modulators thymol and carvacrol, which are suggested to bind at a transmembrane site (Lansdell et al., 2014) (Fig. 4A). Figure 4B shows the standard recording protocol used to compare the ΔF induced by different ligands. Briefly, the protocol employs an initial application of 100 μM 5-HT followed by a washout period to allow full recovery from desensitization of the receptors before the application of test ligand. Controls for

Molecular Pharmacology Fast Forward. Published on October 3, 2019 as DOI: 10.1124/mol.119.116657
This article has not been copyedited and formatted. The final version may differ from this version.

non-specific effects of ligands on TAMRA fluorescence included experiments on oocytes expressing WT h5-HT_{3A} or uninjected oocytes subjected to similar MTS-TAMRA labeling protocols (*Supplementary Fig. S3*). These showed that saturating concentrations of all ligands evoked less than 1 % ΔF at labeled uninjected or WT h5-HT_{3A} expressing oocytes, except for thymol and carvacrol which at 1 mM caused decreasing ΔF in the -1 to -3% range at both uninjected and WT expressing oocytes. However, these differences were considered small relative to the 5-HT induced fluorescence changes at the reporter positions, and thus thymol and carvacrol were characterized for ΔF at the reporter positions.

Ligand-specific fluorescence signals for the loop D mutant Y89C – Tyr89 is located on loop D, which is part of a *β*-sheet motif forming the back wall of the orthosteric binding site (Fig. 3). For this reporter position, all tested ligands displayed ΔF responses to application of saturating concentrations that were very similar in amplitude and direction as the ΔF observed for 5-HT; except for thymol and carvacrol, which did not evoke detectable specific ΔF (Fig. 4C). Figure 5A summarizes the amplitude pattern of the ligand-specific ΔF responses normalized to the response amplitude of the ΔF to evoked by saturating concentration of 5-HT. The orthosteric ligands mCPBG, granisetron, ondansetron, tropisetron, and encenicline all induced ΔF with amplitudes that were not significantly different from those induced by 5-HT (Fig. 5A). These results indicate that the local environment surrounding loop D may experience similar changes in physiochemical properties in response to binding of orthosteric agonists and competitive antagonists.

Ligand-specific fluorescence signals for the loop E mutant Q146C – Gln146 is located on loop E, which like loop D forms part of the *β*-sheet at the back of the binding site (Fig. 3). All ligands tested at the TAMRA-labelled Q146C mutant caused robust increases in TAMRA fluorescence upon application, except thymol and carvacrol that did not induce specific ΔF (Fig. 5B). 5-HT and the synthetic agonist mCPBG induced similar ΔF values, suggesting that both agonists induce

similar local conformational changes around loop E upon binding and receptor activation. In contrast, all antagonists induced ΔF that was significantly larger than 5-HT (300 to 600%; Fig. 4B and 5B). Q146C, therefore, appears to report the regions around loop E to undergo conformational changes upon orthosteric ligand binding that are distinct for agonists and antagonists.

Ligand-specific fluorescence signals for the loop C mutant M223C – Met223 is located on loop C (Fig. 3), a region on the principal subunit which is thought to be flexible and adopt a contracted conformation upon agonist binding and an extended conformation when antagonists are bound (Kesters et al., 2012; Polovinkin et al., 2018). At TAMRA-labeled M223C mutant 5-HT_{3A} receptors, all tested ligands reported an ΔF in the same direction as 5-HT (Fig. 4E). However, in contrast to the relative ΔF patterns observed at the Y89C and Q146C mutant receptors, there was no clear trend in terms of the relative amplitude of the ΔF values for agonist or antagonist or positive allosteric modulators (Fig. 5C). mCPBG displayed ΔF values that were 34% of those for 5-HT (Fig. 5C). For the four antagonists, ondansetron and encenicline induced ΔF that were 70 to 130% larger than 5-HT, respectively, whereas granisetron and tropisetron displayed similar ΔF compared to the 5-HT application. Thymol and carvacrol evoked currents of similar amplitude as 5-HT, and both caused a small, but significant ΔF with amplitudes of 22% and 15%, respectively, of the 5-HT evoked ΔF (Fig. 4E and 5C).

Concentration-response relationship of ligand-specific fluorescence signals - The robust ligand-evoked ΔF responses for Y89C, Q146C, and M223C allowed the determination of steady-state concentration-response relationships for the fluorescence responses (Fig. 6, Table 2). Importantly, this enabled us to determine the EC_{50} of the ΔF response for the electrically silent process of antagonist binding (Table 3). At Y89C receptors for the endogenous agonist 5-HT, we found that the fluorescence EC_{50} was increased by approximately 6-fold compared to the EC_{50} obtained from the simultaneously determined current responses (Table 2). A similar result was obtained for the

Molecular Pharmacology Fast Forward. Published on October 3, 2019 as DOI: 10.1124/mol.119.116657
This article has not been copyedited and formatted. The final version may differ from this version.

agonist mCPBG, which displayed a 4-fold increase in the EC_{50} for ΔF responses compared to the EC_{50} obtained from current responses (Table 2). M223C receptors reported similar EC_{50} values for current and ΔF in response to 5-HT, while mCPBG exhibited an EC_{50} of ΔF responses that were approximately 2.5-fold larger than current responses (Table 2). Q146C receptors showed the largest difference between fluorescence and current responses with 5-HT and mCPBG showing EC_{50} values for fluorescence responses that were 12- and 45-fold larger than the EC_{50} values for current responses, respectively (Table 2). The concentration-response relationship for ΔF signals induced by the competitive antagonists granisetron, ondansetron, tropisetron, and encenicline showed ΔF response amplitudes to be concentration-dependent (Fig. 6). In general, the obtained EC_{50} values for ΔF were within 10-fold range of previously reported IC_{50} or K_d values for all of the antagonists (Hope et al., 1996; Lankiewicz et al., 1998; Ladefoged et al., 2018); except for the Q146C mutant that displayed decreased EC_{50} values for ΔF compared to Y89C and M223C mutants, which suggest that Cys-mutation and/or TAMRA conjugation decreases ligand affinity. In general, we did not attempt to quantify the rate by which the fluorescence signal decayed back towards baseline during the ligand post-application wash-out phase due to the design of our VCF recording chamber which did not allow for solution exchange rates likely required to isolate the rate of ensemble receptor transitions upon removal of extracellular ligand. However, it is interesting to note that the fluorescence response at Q146C for ligands such as encenicline and ondansetron consistently decreased much faster during the wash-out phase compared to the responses at Y89C and M223C (Fig. 4C-D); indicating that the ligand dissociation rate at TAMRA-labeled Q146C may be increased.

Molecular Pharmacology Fast Forward. Published on October 3, 2019 as DOI: 10.1124/mol.119.116657
This article has not been copyedited and formatted. The final version may differ from this version.

8. Discussion

Crystal and cryo-EM structures of the m5-HT_{3A} receptor (Hassaine et al., 2014; Basak et al., 2018a; Polovinkin et al., 2018; Basak et al., 2018b; Basak et al., 2019) and other Cys-loop receptors (Du et al., 2015; Morales-Perez et al., 2016; Phulera et al., 2018) have established structural conformations that likely reflect key functional receptor states, and thereby provide an essential framework for beginning to understand the structural mechanism of the 5-HT_3 receptor. However, as static structures, these do not provide direct evidence for specific protein motions that occur during receptor state transitions. In our present study, we have used VCF to study conformational changes in the h5-HT_{3A} receptor to provide direct experimental evidence of structural changes around the orthosteric ligand binding site of the h5-HT_{3A} receptor during ligand binding and channel activation. We identify positions in loop C, D, and E where measurement of fluorescence from a conjugated environmentally sensitive fluorophore allow tracking of conformational changes in response to binding of a range of prototypical 5-HT_3 ligands; including the endogenous agonist 5-HT. Interpretation of our fluorescence data in the context of presently available Cys-loop receptor structures presents an opportunity to evaluate and expand current structure-based models for the early steps in the 5-HT_3 receptor activation mechanism. Specifically, the comparison of the patterns of fluorescence changes induced by different ligands provides insight into the differences in conformational changes that underlie agonist and antagonist ligand function. However, a potential concern for interpreting changes in fluorescence from the reporter fluorophore as the results of protein rearrangements is whether the fluorophore microenvironment is affected directly by the proximity of the bound ligands. In terms of direct ligand effects that produce decreases in fluorescence, examples include resonance energy transfer to the ligand or simple absorbance of emitted light by the ligand (Unruh et al., 2005; Pless & Lynch, 2009b; Talwar & Lynch, 2015). However, none of the ligands induce decreases in TAMRA fluorescence (Fig. 4C and 5), and such

Molecular Pharmacology Fast Forward. Published on October 3, 2019 as DOI: 10.1124/mol.119.116657
This article has not been copyedited and formatted. The final version may differ from this version.

direct quenching effects are therefore not a concern in the present study. Direct ligand effects that increase fluorescence require that the presence of the ligand changes the physicochemical microenvironment around the fluorophore such that its quantum yield is increased. In the case of TAMRA, this most likely means increasing overall hydrophobicity; for example, by shielding the fluorophore from polar protein structure elements or water molecules or by direct steric effects that promote the fluorophore to orient towards a more hydrophobic environment. In this context, we observe that our modeling of TAMRA conjugated to the Cys-mutated Tyr89, and Gln146 positions in the h5-HT_{3A} receptor show that the fluorophore in these positions cannot access the binding site, and thus not be in direct contact with ligands (Fig. 3B and C). In contrast, for the Met223 position, the side chain of the inserted Cys residue is facing into the binding pocket (Fig. 3D), and the accessible volume calculations show that TAMRA from this position can at least partially occupy the binding pocket and thus potentially experience direct effects of orthosteric ligands; an aspect that therefore must be taken into concern for interpretation of the ΔF reported from this position. Another important issue for interpreting fluorescence data is that we utilize a steady-state recording methodology on a time-scale that does not allow us to resolve receptor transitions (e.g. *apo* to pre-active, active to desensitized); meaning that we cannot know whether a change in fluorescence is due to a local conformational change, such as a localized rearrangement of the orthosteric binding site upon ligand binding, or global conformational changes underlying transitions between receptor functional states.

At positions 89 and 146 in the D and the E loop, respectively, the conjugated TAMRA consistently showed increases in fluorescence upon binding of all the tested orthosteric ligands; thus, showing that conformational changes occur around these positions upon ligand binding. Principally, these changes can involve the local rearrangement of loop D and E, as well as the surrounding protein regions. Regarding the possibility of direct loop movements as a source for ΔF,

Molecular Pharmacology Fast Forward. Published on October 3, 2019 as DOI: 10.1124/mol.119.116657
This article has not been copyedited and formatted. The final version may differ from this version.

then both loop E and D, together with loop G, form strands in a *β*-sheet structure that lines the back of the orthosteric binding site. This *β*-sheet motif is considered to be rigid, and comparison of its conformation in recent structures of m5-HT_{3A} and other Cys-loop receptors suggest it to undergo little or no overall structural rearrangement during receptor state transitions (Nys et al., 2013; Hassaine et al., 2014; Du et al., 2015; Basak et al., 2018a; Polovinkin et al., 2018; Basak et al., 2018b; Basak et al., 2019). Thus, it appears more likely that TAMRA at both positions reports movement of surrounding structural elements. Candidate elements that might influence fluorescence from TAMRA conjugated at loop E and D first and foremost include the C loop, which is positioned in close vicinity of both positions (Fig. 3). This is based on long-standing models for Cys-loop receptor function that involves the idea that ligand binding induces local movement of loop C around the orthosteric binding site (Chang & Weiss, 2002; Law et al., 2005; Pless & Lynch, 2009b; Kesters et al., 2012; Puruhit & Auerbach, 2013; Du et al., 2015). However, for the reporter position 89, potential structural rearrangement of loop F is also a possible candidate and this loop region contains several residues that are suggested to be directly involved in agonist recognition (Thompson et al., 2006) and assumes different conformations among the presently available 5-HT_3 receptor structures (Hassaine et al., 2014; Basak et al., 2018a; Polovinkin et al., 2018; Basak et al., 2018b; Basak et al., 2019). Likewise, the reporter position 146 may be influenced by movements of loop B. Interestingly, although the *N*-terminal segment of loop B is locked in a *β*-strand motif and likely is overall rigid during state transitions, the *C*-terminal region is not and may be able to adapt locally to ligand binding (Fig. 1A). Overall, this idea is supported by comparison of structures of *apo* and 5-HT bound 5-HT_{3A} which show the ECD to adopt a more condensed conformation with 5-HT bound; most pronounced around the lower half of the ECD and loops B and C (Polovinkin et al., 2018; Basak et al., 2018b). In addition, a recent structure of 5-

Molecular Pharmacology Fast Forward. Published on October 3, 2019 as DOI: 10.1124/mol.119.116657
This article has not been copyedited and formatted. The final version may differ from this version.

HT_{3A} in complex with the antagonist granisetron also shows the ECD to condense when granisetron is bound; including a shift in the positions of loop B and C (Basak et al., 2019).

In contrast to the distinctly different levels of ligand-induced ΔF for agonist and antagonists observed at the Q146C mutant, the Y89C mutant reported strikingly similar levels of ΔF for both agonists and competitive antagonists. This potentially means that if TAMRA conjugated to position 89 in loop D senses ligand-induced conformational changes, then these are distinct from those reported by TAMRA at position 146; despite the two reporter positions being closely located in the binding site (Fig. 3A). However, it should be noted that it is possible that different rearrangement upon agonist and antagonist binding can produce similar net effects on the environment around TAMRA and thus similar changes in fluorescence. Also, ligand binding may induce changes to the environment around TAMRA that are not directly related to conformational changes. Notably, albeit the accessible volume calculations show substantial overlap in the parts of the receptor surface that TAMRA can sample for both positions, only TAMRA at position 89 can sample the surface near loop D in the back of the pocket (Fig. 3B and 3C). Instead of conformational changes, a possible source for the similar fluorescence response by the Y89C mutant to agonists and antagonists can be that ligand occupation of the binding pocket, in general, displaces one or more water molecules to increase general hydrophobicity and enhance TAMRA fluorescence.

Comparison of the ΔF observed at the Q146C mutant for agonists with those observed for antagonists shows a striking pattern where the agonists 5-HT and mCPBG induce similar ΔF, whereas the four competitive antagonists induce a distinct set of ΔF of likewise similar magnitude (Fig. 5B). VCF studies on other Cys-loop receptors have labeled positions in loop E and compared the effects of agonists and antagonists (Muroi et al., 2006; Pless & Lynch, 2009b; Akk et al., 2011). In $GABA_A$ receptors, Akk et al. (2011) observed that a fluorophore-labeled loop E position, corresponding to Gln146 in h5-HT_{3A}, reported increases in fluorescence that were several-fold

Molecular Pharmacology Fast Forward. Published on October 3, 2019 as DOI: 10.1124/mol.119.116657
This article has not been copyedited and formatted. The final version may differ from this version.

larger in amplitude for the competitive antagonist gabazine than for the orthosteric agonists GABA and muscimol. Also, at the $GABA_A$ receptor, Chang et al. (2002) found that loop E position corresponding to position Gln146 in h5-HT_{3A} reported distinct fluorescence changes for GABA and the competitive antagonist 3-APMPA. Similarly, in glycine α1 receptors, Pless *et al.* (2009) reported that a loop E reporter position, which corresponds to Gln146 in h5-HT_{3A} receptors (*Supplementary Fig S1*; Table 1), showed a greater increase in fluorescence in response to the competitive antagonist strychnine than to the agonist glycine. Taken together with the results from the present study, which utilized a wider range of competitive antagonists, loop E of Cys-loop receptors seems to consistently report VCF results which reflect the functional properties of the ligand. Distinct conformational changes around loop E may thus be a hallmark feature of Cys-loop receptor agonism versus antagonism.

Met223 is located in loop C, and changes in fluorescence for TAMRA conjugated at this position might be ideal for tracking of movement of loop C during ligand binding as well as the ECD tightening occurring during receptor activation; due to its close proximity to the interface of the principal and the complementary subunit of each binding site. At this position, we did observe fluorescence changes for all ligands, but these displayed a range of relative ΔF magnitudes that did not follow any pattern correlated to ligand functionality (Fig. 5C). Movement of Loop C has been proposed a central role in mechanistic models for Cys-loop receptor function. Specifically, binding of ligands that act as agonists have been proposed to contract loop C around the orthosteric binding site, while binding of ligands that act as antagonist do not induce constriction or induce a more extended orientation compared to the *apo* state (Celie et al., 2004; Hansen et al., 2005; Brams et al., 2011, Kesters et al., 2012; Alix et al., 2016). This "capping" movement by loop C has been proposed essential for promoting structural transitions towards the opening of the channel gate; either via a global transition or a sequence of local conformational changes of neighboring domains

Molecular Pharmacology Fast Forward. Published on October 3, 2019 as DOI: 10.1124/mol.119.116657
This article has not been copyedited and formatted. The final version may differ from this version.

that eventually reach the channel gate. However, another model is that the varying loop C conformations in ligand-bound structures reflect the role of loop C residues in forming contacts with the ligand (Purohit & Auerbach, 2013). In this model, loop C "capping" correlates with activation not by inducing conformational change, but by local stabilization of the binding site in a conformation with high open probability. For the $5HT_{3A}$ receptor, these ideas can now be evaluated by a series of structures of the m5-HT_{3A} receptor in the *apo* state and in complex with 5-HT (Polovinkin et al., 2018; Basak et al., 2018b) and the antagonist tropisetron and granisetron (Basak et al., 2019). Comparison of the orientation of the C loop between *apo* and 5-HT bound structures indeed show that the C loop contracts around the orthosteric binding; moving towards loop E and D, whereas the orientation of loop C in the tropisetron-bound structure closely resembles the *apo* orientation; hereby supporting the model with loop C contraction as a key conformational change for receptor activation. However, the granisetron-bound structure also shows contraction of loop C around the binding site that is similar in direction with the 5-HT bound structure; although 5-HT appears to induce most contraction (Basak et al., 2019). We find binding of 5-HT, granisetron, and tropisetron to all produce increases in fluorescence from TAMRA conjugated to position 223 in loop C; with 5-HT and granisetron producing identical responses that are slightly higher in magnitude than tropisetron (Fig. 5B). Overall, these results suggest that loop C is closing around these ligands, which potentially indicate a more complex role of loop C movement for receptor activation or inhibition than suggested by the aforementioned existing models. However, as discussed previously, a significant concern is that TAMRA at position 223 may occupy the binding pocket and thus experience direct effects from ligand binding. Thus, further work is needed to explore other loop C positions that do not allow the fluorophore to potentially occupy the binding pocket while serving as reporters for loop C movement in the 5-HT_3 receptor as well as the arrival of structures of 5-HT_{3A} in complex with additional agonists and antagonists.

Molecular Pharmacology Fast Forward. Published on October 3, 2019 as DOI: 10.1124/mol.119.116657
This article has not been copyedited and formatted. The final version may differ from this version.

Thymol and carvacrol are structurally closely related positive allosteric modulators of the h5-HT_{3A} receptor. Their binding site is proposed to be located in the transmembrane domain at the subunit interface (Lansdell et al., 2014), which also has been suggested as the binding site for the positive allosteric modulator TMPPAA (Gasiorek et al., 2016; Polovinkin et al., 2018) not explored in the present study. The M223C mutant showed slight, but significant increases in fluorescence in response to both compounds (Fig. 5). As M223C is located on loop C, which connects directly into the TMD region, this result may demonstrate the allosteric coupling between the orthosteric site and the conformational changes that underlie channel activation as has previously been proposed (Du et al., 2015).

In summary, we have established a VCF approach for studies of conformational changes in the ECD region of the h5-HT_{3A} receptor that contains the orthosteric binding site. We utilize this to compare the conformational effects of different classes of 5-HT_3 receptor ligands to define various ligand-specific aspects of ligand binding. First, consistent with current predictions from structural and biochemical studies, our results support the idea that agonists and competitive antagonists induce distinct conformational changes in the orthosteric binding site. Second, the nature of the ligand-induced conformational changes around loop E appears to be a determinant for ligand functionality as either agonist or antagonist most likely by assessing the inter-subunit tightness in the ECD. Overall, our observations hereby provide insight into the initial steps of the conformational cycle that underlies the ligand-gated ion channel function of the 5-HT_3 receptor. We note that we were not successful in identifying reporter positions that could report structural transitions outside the immediate ECD regions containing the orthosteric binding site. VCF work focused on identifying useful reporter positions in the ECD/TMD interfaces is therefore warranted to enable tracking of structural changes further into the receptor functional cycle. Whereas our present work focused on the ECD segment, it is in this respect encouraging to note that recent work

Molecular Pharmacology Fast Forward. Published on October 3, 2019 as DOI: 10.1124/mol.119.116657
This article has not been copyedited and formatted. The final version may differ from this version.

on the m5-HT_{3A} receptor has reported a position (Ser296) in the upper region of the pore-lining M2 helix as a useful VCF reporter for structural rearrangements associated with gating transition (Polovinkin et al., 2018).

Molecular Pharmacology Fast Forward. Published on October 3, 2019 as DOI: 10.1124/mol.119.116657
This article has not been copyedited and formatted. The final version may differ from this version.

9. Authorship Contribution

Participated in research design: Munro, Ladefoged, Schiøtt, and Kristensen.

Conducted experiments: Munro, Andersen, Padmanathan, Ladefoged, and Kristensen.

Performed data analysis: Munro, Ladefoged, and Kristensen.

Wrote or contributed to the writing of the manuscript: Munro, Ladefoged, Schiøtt, and Kristensen.

10. References

Akk G, Li P, Bracamontes J, Wang M, and Steinbach JH (2011) Pharmacology of structural changes at the GABAAreceptor transmitter binding site. *Br J Pharmacol* **162**:840–850.

Alix K, Khatri S, Mosier PD, Casterlow S, Yan D, Nyce HL, White MM, Schulte MK, and Dukat M (2016) Superagonist, Full Agonist, Partial Agonist, and Antagonist Actions of Arylguanidines at 5-Hydroxytryptamine-3 (5-HT3) Subunit A Receptors. *ACS Chem Neurosci* **7**:1565–1574.

Barnes NM, Hales TG, Lummis SCR, and Peters JA (2009) The 5-HT3receptor - the relationship between structure and function. *Neuropharmacology* **56**:273–284.

Basak S, Gicheru Y, Kapoor A, Mayer ML, Filizola M and Chakrapani S (2019) Molecular mechanism of setron-mediated inhibition of full-length 5-HT3A receptor. *Nat Commun* **10**(1): 3225.

Basak S, Gicheru Y, Rao S, Sansom MSP, and Chakrapani S (2018a) Cryo-EM reveals two distinct serotonin-bound conformations of full-length 5-HT_{3A} receptor. *Nature* **563**:270–274.

Basak S, Gicheru Y, Samanta A, Molugu SK, Huang W, Fuente ML De, Hughes T, Taylor DJ, Nieman MT, Moiseenkova-Bell V, and Chakrapani S (2018b) Cryo-EM structure of 5-HT_{3A} receptor in its resting conformation. *Nat Commun* **9**:514.

Brejc K, Van Dijk WJ, Klaassen R V., Schuurmans M, Van Der Oost J, Smit AB, and Sixma TK (2001) Crystal structure of an ACh-binding protein reveals the ligand-binding domain of nicotinic receptors. *Nature* **411**:269–276.

Castaldo P, Stefanoni P, Miceli F, Coppola G, Del Giudice EM, Bellini G, Pascotto A, Trudell JR, Harrison NL, Annunziato L and Taglialatela M (2004) A novel hyperekplexia-causing mutation in the pre-transmembrane segment 1 of the human glycine receptor alpha1 subunit reduces membrane expression and impairs gating by agonists. *J Biol Chem* **279**(24): 25598-

25604.

Celie PH, van Rossum-Fikkert SE, van Dijk WJ, Brejc K, Smit AB, Sixma TK (2004) Nicotine and carbamylcholine binding to nicotinic acetylcholine receptors as studied in AChBP crystal structures. *Neuron* **41**(6):907-14.

Chang Y, and Weiss DS (2002) Site-specific fluorescence reveals distinct structural changes with GABA receptor activation and antagonism. *Nat Neurosci* **5**:1163–1168.

Corringer PJ, Baaden M, Bocquet N, Delarue M, Dufresne V, Nury H, Prevost M, and Van Renterghem C (2010) Atomic structure and dynamics of pentameric ligand-gated ion channels: New insight from bacterial homologues. *J Physiol* **588**:565–572.

Dahan DS, Dibas MI, Petersson EJ, Auyeung VC, Chanda B, Bezanilla F, Dougherty DA, and Lester HA (2004) A fluorophore attached to nicotinic acetylcholine receptor beta M2 detects productive binding of agonist to the alpha delta site. *Proc Natl Acad Sci* **101**:10195–10200.

Davies PA, Pistis M, Hanna MC, Peters JA, Lambert JJ, Hales TG and Kirkness EF (1999) The 5-HT3B subunit is a major determinant of serotonin-receptor function. *Nature* **397**(6717): 359-363.

Du J, Lü W, Wu S, Cheng Y, and Gouaux E (2015) Glycine receptor mechanism elucidated by electron cryo-microscopy. *Nature* **526**:224–229.

Du J, Dong H and Zhou HX (2012) Size matters in activation/inhibition of ligand-gated ion channels. *Trends Pharmacol Sci* **33**(9): 482-493.

Dubin AE, Huvar R, D'Andrea MR, Pyati J, Zhu JY, Joy KC, Wilson SJ, Galindo JE, Glass CA, Luo L, Jackson MR, Lovenberg TW and Erlander MG (1999) The pharmacological and functional characteristics of the serotonin 5-HT(3A) receptor are specifically modified by a 5-HT(3B) receptor subunit. *J Biol Chem* **274**(43): 30799-30810.

Eaton MM, Lim Y Bin, Covey DF, and Akk G (2014) Modulation of the human ρ1 GABAA

receptor by inhibitory steroids. *Psychopharmacology (Berl)* **231**:3467–3478.

Gasiorek A, Trattnig SM, Ahring PK, Kristiansen U, Frølund B, Frederiksen K, and Jensen AA (2016) Delineation of the functional properties and the mechanism of action of TMPPAA, an allosteric agonist and positive allosteric modulator of 5-HT3 receptors. *Biochem Pharmacol* **110–111**:92–108.

Greenwood JR, Calkins D, Sullivan AP, and Shelley JC (2010) Towards the comprehensive, rapid, and accurate prediction of the favorable tautomeric states of drug-like molecules in aqueous solution. *J Comput Aided Mol Des* **24**:591–604.

Grosman C, Zhou M, and Auerbach A (2000) Mapping the conformational wave of acetylcholine receptor channel gating. *Nature* **403**:773–776.

Hansen SB, Sulzenbacher G, Huxford T, Marchot P, Taylor P and Bourne Y (2005) Structures of Aplysia AChBP complexes with nicotinic agonists and antagonists reveal distinctive binding interfaces and conformations. *EMBO J* **24**(20): 3635-3646.

Hassaine G, Deluz C, Grasso L, Wyss R, Tol MB, Hovius R, Graff A, Stahlberg H, Tomizaki T, Desmyter A, Moreau C, Li X-D, Poitevin F, Vogel H, and Nury H (2014) X-ray structure of the mouse serotonin 5-HT3 receptor. *Nature* **512**:276–281.

Hope AG, Peters JA, Brown AM, Lambert JJ, and Blackburn TP (1996) Characterization of a human 5-hydroxytryptamine3receptor type A (h5-HT3R-A(s)) subunit stably expressed in HEK 293 cells. *Br J Pharmacol* **118**:1237–1245.

Joshi PR, Suryanarayanan A and Schulte MK (2004) A vertical flow chamber for Xenopus oocyte electrophysiology and automated drug screening. *J Neurosci Methods* **132**(1): 69-79.

Kalinin S, Peulen T, Sindbert S, Rothwell PJ, Berger S, Restle T, Goody RS, Gohlke H, and Seidel CAM (2012) A toolkit and benchmark study for FRET-restrained high-precision structural modeling. *Nat Methods* **9**:1218–1225.

Keramidas A1, Lynch JW (2013) An outline of desensitization in pentameric ligand-gated ion channel receptors. *Cell Mol Life Sci* **70**:1241-53.

Kesters D, Thompson AJ, Brams M, van Elk R, Spurny R, Geitmann M, Villalgordo JM, Guskov A, Helena Danielson U, Lummis SCR, Smit AB, and Ulens C (2012) Structural basis of ligand recognition in 5-HT3 receptors. *EMBO Rep* **14**:49–56.

Khatri A, Sedelnikova A, and Weiss DS (2009) Structural rearrangements in loop F of the GABA receptor signal ligand binding, not channel activation. *Biophys J* **96**:45–55.

Kilpatrick GJ, Butler A, Burridge J, and Oxford AW (1990) 1-(m-Chlorophenyl)-biguanide, a potent high affinity 5-HT3 receptor agonist. *Eur J Pharmacol* **182**:193–197.

Ladefoged LK, Munro L, Pedersen AJ, Balle T, Bang-Andersen B, Lummis SCR, Schiott B, and Kristensen AS (2018) Modeling and mutational analysis of the binding mode for the multimodal antidepressant drug vortioxetine to the human 5-HT3A receptor. *Mol Pharmacol* **94**:1421–1434.

Lankiewicz S, Lobitz N, Wetzel CHR, Rupprecht R, Unter G, and Hatt H (1998) Molecular Cloning, Functional Expression, and Receptor cDNA and Its Splice Variants from Guinea Pig. *Mol Pharmacol*. **53**(2):202-12.

Lansdell SJ, Sathyaprakash C, Doward A, and Millar NS (2014) Activation of Human 5-Hydroxytryptamine Type 3 Receptors via an Allosteric Transmembrane Site. *Mol Pharmacol* **87**:87–95.

Law RJ, Henchman RH, and McCammon JA (2005) A gating mechanism proposed from a simulation of a human 7 nicotinic acetylcholine receptor. *Proc Natl Acad Sci* **102**:6813–6818.

Lummis SCR (2012) 5-HT3 receptors. *J Biol Chem* **287**:40239–40245.

Lynagh T, and Lynch JW (2012) Molecular mechanisms of Cys-loop ion channel receptor modulation by ivermectin. *Front Mol Neurosci* **5**:1–11.

Mannuzzu LM, Moronne MM, and Isacoff EY (1996) Direct physical measure of conformational rearrangement underlying potassium channel gating. *Science* **271**:213–216.

Menny A, Lefebvre SN, Schmidpeter PA, Drege E, Fourati Z, Delarue M, Edelstein SJ, Nimigean CM, Joseph D and Corringer PJ (2017) Identification of a pre-active conformation of a pentameric channel receptor. *Elife* **15**:e23955

Morales-Perez CL, Noviello CM, and Hibbs RE (2016) X-ray structure of the human α4β2 nicotinic receptor. *Nature* **538**:411–415.

Muroi Y, Czajkowski C, and Jackson MB (2006) Local and global ligand-induced changes in the structure of the GABA A receptor. *Biochemistry* **45**:7013–7022.

Muroi Y, Theusch CM, Czajkowski C, and Jackson MB (2009) Distinct structural changes in the GABA A receptor elicited by pentobarbital and GABA. *Biophys J* **96**:499–509.

Mourot A, Bamberg E and Rettinger J (2008) Agonist- and competitive antagonist-induced movement of loop 5 on the alpha subunit of the neuronal alpha4beta4 nicotinic acetylcholine receptor. *J Neurochem* **105**(2): 413-424.

Nemecz Á, Prevost MS, Menny A, and Corringer PJ (2016) Emerging Molecular Mechanisms of Signal Transduction in Pentameric Ligand-Gated Ion Channels. *Neuron* **90**:452–470.

Nys M, Kesters D, and Ulens C (2013) Structural insights into Cys-loop receptor function and ligand recognition. *Biochem Pharmacol* **86**:1042–1053.

Phulera S, Zhu H, Yu J, Claxton DP, Yoder N, Yoshioka C, and Gouaux E (2018) Cryo-EM structure of the benzodiazepine-sensitive α1β1γ2S tri-heteromeric GABAAreceptor in complex with GABA. *Elife* **7**:1–21.

Pless SA, and Lynch JW (2009a) Distinct conformational changes in activated agonist-bound and agonist-free glycine receptor subunits. *J Neurochem* **108**:1585–1594.

Pless SA, and Lynch JW (2009b) Ligand-specific conformational changes in the alpha1 glycine

receptor ligand-binding domain. *J Biol Chem* **284**:15847–15856.

Polovinkin L, Hassaine G, Perot J, Neumann E, Jensen AA, Lefebvre SN, Corringer PJ, Neyton J, Chipot C, Dehez F, Schoehn G, and Nury H (2018) Conformational transitions of the serotonin 5-HT3 receptor. *Nature* **563**:275–279.

Poulsen MH, Lucas S, Stromgaard K, and Kristensen AS (2014) Evaluation of PhTX-74 as Subtype-Selective Inhibitor of GluA2-Containing AMPA Receptors. *Mol Pharmacol* **85**:261-268.

Price KL, Lillestol RK, Ulens C, and Lummis SCR (2016) Palonosetron-5-HT3 Receptor Interactions As Shown by a Binding Protein Cocrystal Structure. *ACS Chem Neurosci* **7**:1641–1646.

Price KL, Lillestol RK, Ulens C, and Lummis SCR (2015) Varenicline Interactions at the 5-HT $_3$ Receptor Ligand Binding Site are Revealed by 5-HTBP. *ACS Chem Neurosci* **6**:1151–1157.

Purohit P and Auerbach A (2013) Loop C and the mechanism of acetylcholine receptor-channel gating. *J Gen Physiol* **141**(4): 467-478.

Purohit P, Gupta S, Jadey S and Auerbach A (2013) Functional anatomy of an allosteric protein. *Nat Commun* 4: 2984.

Sastry GM, Adzhigirey M, Day T, Annabhimoju R, and Sherman W (2013) Protein and ligand preparation: Parameters, protocols, and influence on virtual screening enrichments. *J Comput Aided Mol Des* **27**:221–234.

Shelley JC, Cholleti A, Frye LL, Greenwood JR, Timlin MR, and Uchimaya M (2007) Epik: A software program for pKa prediction and protonation state generation for drug-like molecules. *J Comput Aided Mol Des* **12**:681–691.

Sixma TK, and Smit AB (2003) Acetylcholine Binding Protein (AChBP): A Secreted Glial Protein That Provides a High-Resolution Model for the Extracellular Domain of Pentameric Ligand-

Gated Ion Channels. *Annu Rev Biophys Biomol Struct* **32**:311–334.

Soderhielm PC, Andersen J, Munro L, Nielsen AT, and Kristensen AS (2015) Substrate and Inhibitor-Specific Conformational Changes in the Human Serotonin Transporter Revealed by Voltage-Clamp Fluorometry. *Mol Pharmacol* **88**:676–688.

Soh MS, Estrada-Mondragon A, Durisic N, Keramidas A, and Lynch JW (2017) Probing the Structural Mechanism of Partial Agonism in Glycine Receptors Using the Fluorescent Artificial Amino Acid, ANAP. *ACS Chem Biol* **12**:805–813.

Talwar S, and Lynch JW (2015) Investigating ion channel conformational changes using voltage clamp fluorometry. *Neuropharmacology* **98**:3–12.

Thompson AJ, and Lummis SC (2007) The 5-HT 3 receptor as a therapeutic target. *Expert Opin Ther Targets* **11**:527–540.

Thompson AJ, Padgett CL, and Lummis SCR (2006) Mutagenesis and molecular modeling reveal the importance of the 5-HT 3 receptor F-loop. *J Biol Chem* **281**:16576–16582.

Unruh JR, Gokulrangan G, Wilson GS, and Johnson CK (2005) Fluorescence Properties of Fluorescein, Tetramethylrhodamine, and Texas Red linked to a DNA Aptamer. *Photochem Photobiol* **81**:682–690.

Walstab J, Rappold G, and Niesler B (2010) 5-HT3 receptors: Role in disease and target of drugs. *Pharmacol Ther* **128**:146–169.

Zhang J, Xue F, and Chang Y (2009) Agonist- and antagonist-induced conformational changes of loop F and their contributions to the ρ1 GABA receptor function. *J Physiol* **587**:139–153.

Molecular Pharmacology Fast Forward. Published on October 3, 2019 as DOI: 10.1124/mol.119.116657
This article has not been copyedited and formatted. The final version may differ from this version.

11. Footnotes

This work was supported by the Danish Council of Independent Research for Medical Sciences (grant number DFF-404-00309), the Lundbeck Foundation (grant number 2017-1655 and 2012-12453), and the Carlsberg Foundation. Computations were made possible through allocations at the Centre for Scientific Computing, Arhus (SCS-Aa). We thank Alexander B. J. Jensen for excellent technical assistance.

Molecular Pharmacology Fast Forward. Published on October 3, 2019 as DOI: 10.1124/mol.119.116657
This article has not been copyedited and formatted. The final version may differ from this version.

12. Figure legends

Figure 1. Identification of h5-HT_{3A} residues as voltage-clamp fluorometry reporter positions. ***A***. Surface contoured cartoon representation of a homology model structure of the pentameric h5-HT_{3A} receptor (*left*) from Ladefoged et al. (2018). The principal and complementary subunits are highlighted in *cyan* and *green*, respectively, with indications of the extracellular domain (ECD) and transmembrane domain (TMD). The cross-sectional view (*right*) illustrates the location of the five equivalent 5-HT binding pockets (*dashed circles*) formed at subunit interfaces in the ECD with 5-HT indicated in yellow surface contour. The chemical structure of the endogenous agonist 5-HT is shown below. ***B.*** Zoom of the ECD interface structure in cartoon representation with the orthosteric binding site and the loop A to G regions highlighted in different colors and bound 5-HT in *yellow* surface contour. Positions, where Cys residues were introduced by mutagenesis and the endogenous Cys residues 158 and 171, are indicated as *orange* and *yellow* spheres, respectively. ***C.*** Representative recording traces of parallel fluorescence and current measurements from uninjected oocytes and oocytes expressing WT h5-HT_{3A}, Y89C, Q146C, and M223C mutants during application of 100 μM 5-HT (*black line*). Upper traces (*red*) show the membrane fluorescence signal (F), and lower traces (*black*) show the corresponding membrane currents (I). ***D.*** Summary of fluorescence changes (ΔF) and currents evoked by application of 100 μM 5-HT. Shown are scatter plots of ΔF from individual uninjected oocytes and oocytes injected with WT h5-HT_{3A} or Cys-mutant h5-HT_{3A}. ΔF is calculated as the percentage difference between baseline fluorescence and steady-state fluorescence during 5-HT application (*Material and methods*). Bars represent mean ΔF (± S.E.M): uninjected; -0.71 ± 0.28 (13 oocytes), WT; -0.81 ± 0.23% (22 oocytes), D74C; 1.1 ± 0.3% (9 oocytes), Y89C; 30 ± 2% (77 oocytes), Q146C; 11 ± 1 % (80 oocytes), V196C; -1.2 ± 0.4% (9 oocytes), F221C; 4.6 ± 0.7% (48 oocytes), M223C; 14 ± 1% (83 oocytes), S225C; 1.6 ± 0.6 % (7 oocytes), I238C; 0.63 ± 0.15% (8 oocytes), R239C; 1.8 ± 0.4% (8 oocytes), R241C; 0.39 ±

Molecular Pharmacology Fast Forward. Published on October 3, 2019 as DOI: 10.1124/mol.119.116657
This article has not been copyedited and formatted. The final version may differ from this version.

0.11% (6 oocytes), L243C; -1.8 ± 0.3% (13 oocytes), V246C; 1.1 ± 0.2% (4 oocytes), V247C; 0.66 ± 0.10 (5 oocytes), L249C; 0.56 ± 0.21 (5 oocytes). * Mean response significantly different from WT; $p < 0.05$ (ANOVA with Dunnet's correction for multiple comparisons).

Figure 2. Characterization of effects of Cys-mutation and TAMRA labeling on h5HT$_{3A}$ receptor function. ***A***. Concentration-response curves for 5-HT currents at WT and mutant h5HT$_{3A}$ receptors expressed in oocytes with (*red*) and without (*black*) TAMRA labeling (*Materials and methods*). Data points represent the mean from 3 to 5 independent concentration-response experiments. Error bars are the SEM and are shown when larger than symbol size. ***B***. Superimposed responses to 100-s applications of 1 mM 5-HT (*black bar*) recorded from oocytes injected with the indicated WT or Cys-mutant 5-HT3A subunit mRNA; before (*black traces*) and after TAMRA labeling (*red traces*). The onset of desensitization (*left panels*), activation (*middle panels*) and deactivation (*right panels*) are fitted with mono-exponential functions (*shown as dotted lines*) to determine time constants (τ). Note that for the middle and right panels that show the initial phase of the current response, the superimposed responses are shown on a faster time scale compared to left panel and that amplitudes for all responses are scaled to equal sizes. ***C.*** Summary of time constants for desensitization (τ_{desens}), activation (τ_{act}), and deactivation (τ_{deact}). Data represent the mean and SEM for 5 to 10 oocytes. * Significantly different from unlabeled WT; $p < 0.05$ (ANOVA with Dunnet's correction for multiple comparisons).

Figure 3. Modeling of the orientation of conjugated fluorophores in the h5-HT$_{3A}$ receptor structure. ***A*.** Side view of structural models of TAMRA-conjugation in the mutant Y89C, Q146C, and M223C mutant h5-HT$_{3A}$ receptors. TAMRA is shown in stick representation (*red*) at position 89 in loop D, position 146 in loop E, and position 223 in loop C (*Materials and methods*). The

agonist 5-HT is shown in *yellow* surface contour. ***B-D.*** The predicted accessible volume for TAMRA conjugated at Cys residues inserted at position 89 (***B***), 146 (***C***), and 223 (***D***) are shown in gray as observed frontally from within the membrane (top) as well as from the side (bottom) as calculated by the AV method (*Materials and methods*). The receptor backbone of the principal and complement face of the ECD is shown as light gray ribbons and loops A-F are colored according to the color scheme introduced in Figure 1.

Figure 4. Ligand-induced fluorescence changes in fluorophore-labeled h5-HT$_{3A}$ receptors. ***A.*** Chemical structures of 5-HT$_3$ receptor ligands characterized at the Y89C, Q146C, and M223C reporter mutants. ***B.*** Representative traces illustrating the standard VCF recording protocol for measurement of fluorescence (*F; upper trace in red*) and current (*I; lower trace in black*) responses to ligand application from oocytes expressing h5HT$_{3A}$ reporter mutants (*Materials and methods*). An oocyte expressing the Q146C mutant was exposed 5-HT (*black bar;* 100 μM) followed by a 6 min wash period (*grey bars*) before application of a saturating concentration of encenicline (*blue bar*; 10 μM). Excitation light (*green bars*; 530 nM) was turned off during the wash period to minimize fluorophore photodestruction. Dotted boxes indicate regions of the fluorescence trace that are used for calculation of ΔF for 5-HT and ligand. ***C-D***. Representative parallel fluorescence and current responses to sequential application of 5-HT and ligand (encenicline, 10 μM; ondansetron, 3 μM; granisetron, 3 μM; thymol, 1 mM) at the Y89C (***C***), Q146C (***D***), and M223C (***E***) reporter mutants.

Figure 5. Summary of fluorescence and current response patterns for the Y89C, Q146C, and M223C mutants. ***A-C.*** Graphical summaries of ligand fluorescence response (ΔF_{ligand}) amplitudes normalized to the response amplitude to a previous application of 5-HT ($\Delta F_{5\text{-}HT}$) for the Y89C (***A***), Q146C (***B***), and M223C (***C***) reporter mutants. The 5-HT data represent recordings of a following application of 5-HT following the same standard recording protocol illustrated in Fig.4A. Data

Molecular Pharmacology Fast Forward. Published on October 3, 2019 as DOI: 10.1124/mol.119.116657
This article has not been copyedited and formatted. The final version may differ from this version.

represent mean ± S.E.M. for 5 to 16 recordings of individual oocytes. * Significantly different from 5-HT; $p < 0.05$ (ANOVA with Dunnet's correction for multiple comparisons).

Figure 6. Concentration-response curves for agonist and antagonist-induced fluorescence changes at the Y89C, Q146C, and M223C mutants. ***A.*** Concentration-response curves for fluorescence and current responses evoked by the agonists 5-HT (*upper curves*) and mCPBG (*lower curves*). Data points represent the mean ± SEM from 5 to 8 individual experiments. concentration-dependent increases in fluorescence. ***B.*** Representative traces illustrating the standard recording protocol employed for fluorescence concentration-response experiments. Shown are 5-second segments from recording traces of membrane current (*black traces*) and fluorescence (*red traces*) from an oocyte expressing TAMRA-conjugated Y89C mutant receptor during application of increasing concentrations of ondansetron (*indicated by black bars*) (*Materials & methods*). The excitation LED was pulsed for 200 ms (*indicated by green bars*) every second to limit the fluorophore photodestruction during the extended recording time. Each ligand concentration was applied for two minutes to allow stable fluorescence levels. ***C.*** Concentration-response curves for fluorescence responses evoked by setron-class antagonists at the Y89C, Q146C, and M223C mutants. Data points represent the mean ± SD from 4 to 8 individual experiments.

Molecular Pharmacology Fast Forward. Published on October 3, 2019 as DOI: 10.1124/mol.119.116657
This article has not been copyedited and formatted. The final version may differ from this version.

13. Tables

Table 1: Residues in h5-HT_{3A} selected for cysteine substitution and their equivalents in other Cys-loop receptor subunits previously studied by fluorescence.

Human h5-HT_{3A}	Previously studied positions in Cys-loop receptors as potential VCF reporters			Region
	human ρ1 $GABA_A$	Rat α1 $GABA_A$	Human α1 GlyR	
Asp74[#]	Ser66[a]	*N.T.*	Ala52[d]	Loop 2
Tyr89	*N.T.*	*N.T.*	Gln67[d]	Loop D
Gln146	Leu166[a]	Leu127[c]	Leu127[d]	Loop E
Val196[#]	Asp214[b]	*N.T.*	*N.T.*	Loop F
Phe221	*N.T.*	*N.T.*	*N.T.*	Loop C
Met223	Tyr241[a]	*N.T.*	His201[d]	Loop C
Ser225[#]	*N.T.*	*N.T.*	Asn203[d]	Loop C
Ile238[#]	*N.T.*	*N.T.*	*N.T.*	Pre-M1
Arg239[#]	*N.T.*	*N.T.*	Glu217[d]	Pre-M1
Arg241[#]	*N.T.*	*N.T.*	Gln219[d]	Pre-M1
Leu243[#]	*N.T.*	*N.T.*	Gly221[d]	Pre-M1
Val246[#]	*N.T.*	*N.T.*	Leu224[d]	Pre-M1
Val247[#]	*N.T.*	*N.T.*	Ile225[d]	Pre-M1
Leu249[#]	*N.T.*	*N.T.*	Met227[d]	Pre-M1

[a] Chang *et al.* (2002), [b] Zhang *et al.* (2009), [c] Muroi *et al.* (2006) and [d]Pless & Lynch (2009a). [#] Indicates that the position did not report fluorescence changes when mutated to Cys and labeled with a fluorophore in the indicated study. Residue numbering according to original publications and may differ from canonical sequence numbering. Other studies concerning studies of Cys-loop receptors by fluorescence labeling at other positions thank those in the present study include Mourot *et al*. (2008), Menny *et al*. (2017), and Polovinkin *et al*., (2018). *N. T.*; not tested in the listed subunit.

Molecular Pharmacology Fast Forward. Published on October 3, 2019 as DOI: 10.1124/mol.119.116657
This article has not been copyedited and formatted. The final version may differ from this version.

Table 2: EC_{50} values for current and fluorescence responses to 5-HT and mCPBG at unlabelled and labeled WT and mutant h5-HT_{3A} receptors.

Mutant	5-HT EC_{50}[a] (μM)		mCPGB EC_{50}[a] (μM)	
	TEVC	Δ*F*	*TEVC*	Δ*F*
WT	2.6 [2.2;3.0]	-	0.45 [0.35;0.60]	-
WT + TAMRA	3.5 [3.1;4.7]*	-	0.95 [0.70;1.3]	-
Y89C	0.24 [0.20;0.28]*	-	0.48 [0.34;0.68]	-
Y89C + TAMRA	0.70 [0.56;0.86]*	4.0 [3.2 ; 4.9]#	0.26 [0.20;0.34]	1.0 [0.67;1.5]
Q146C	1.2 [0.9;1.7]*	-	1.5 [1.4;2.0]	-
Q146C + TAMRA	4.8 [3.0;7.9]	61 [48 ; 79]#	1.1 [0.90;1.45]	49 [36;65]#
F221C	85 [76;94]*	-	-	-
F221C + TAMRA	>300*	>300	-	-
M223C	7.2 [5.2;10]*	-	3.7 [3.0;4.5]*	-
M223C + TAMRA	22 [19;26]*	18 [14 ; 23]	8.9 [6.1;13]*	24 [15;38]

[a] EC_{50} values were determined as described in *Methods and materials* by nonlinear fitting of concentration-inhibition data collected at 5 to 10 oocytes. Numbers in bracket denote the 95% confidence interval for EC_{50}. *P <0.01 versus WT. #P <0.01 versus TEVC EC_{50} (ANOVA with Dunnet's correction for multiple comparisons).

Molecular Pharmacology Fast Forward. Published on October 3, 2019 as DOI: 10.1124/mol.119.116657
This article has not been copyedited and formatted. The final version may differ from this version.

Table 3: EC_{50} values for fluorescence responses to antagonists at mutant h5-HT_{3A} receptors.

Reporter mutant	EC_{50}[a] (μM)			
	Ondansetron	Granisetron	Encenicline	Tropisetron
Y89C	58 [36,96]	100 [59;180]	170 [110;270]	45 [24;87]
Q146C	850 [73**;**1000]	800 [670;970]	370 [340;410]	850 [540;1300]
M223C	51 [38;70]	54 [38;77]	74 [59;95]	38 [19;74]

[a] EC_{50} values were determined as described in *Methods and materials* by non-linear fitting of concentration-inhibition data collected at 5 to 10 oocytes. Numbers in bracket denote the 95% confidence interval for EC_{50}.

Molecular Pharmacology Fast Forward. Published on October 3, 2019 as DOI: 10.1124/mol.119.116657
This article has not been copyedited and formatted. The final version may differ from this version.

14. Figures

Figure 1

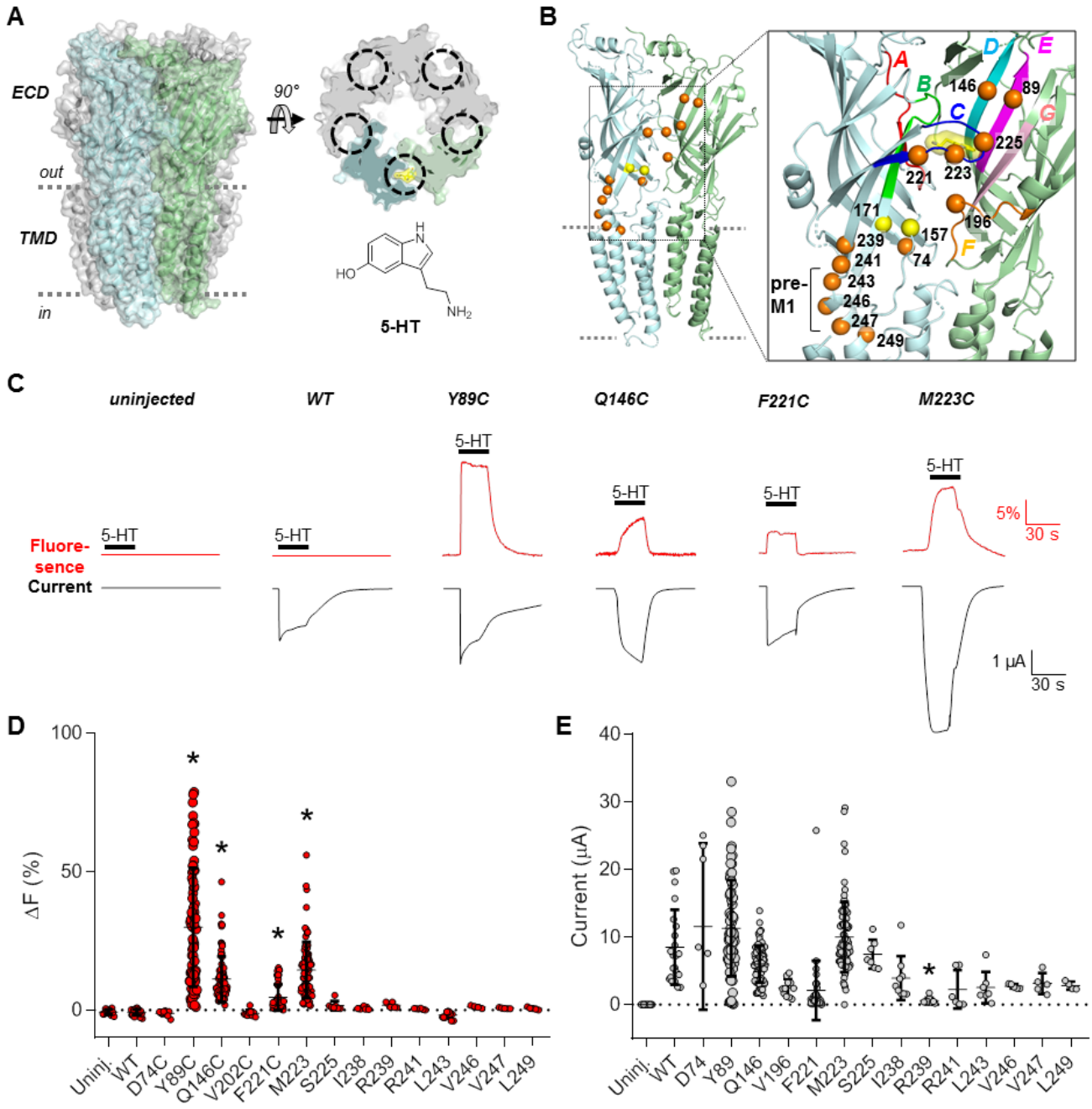

Molecular Pharmacology Fast Forward. Published on October 3, 2019 as DOI: 10.1124/mol.119.116657
This article has not been copyedited and formatted. The final version may differ from this version.

Figure 2

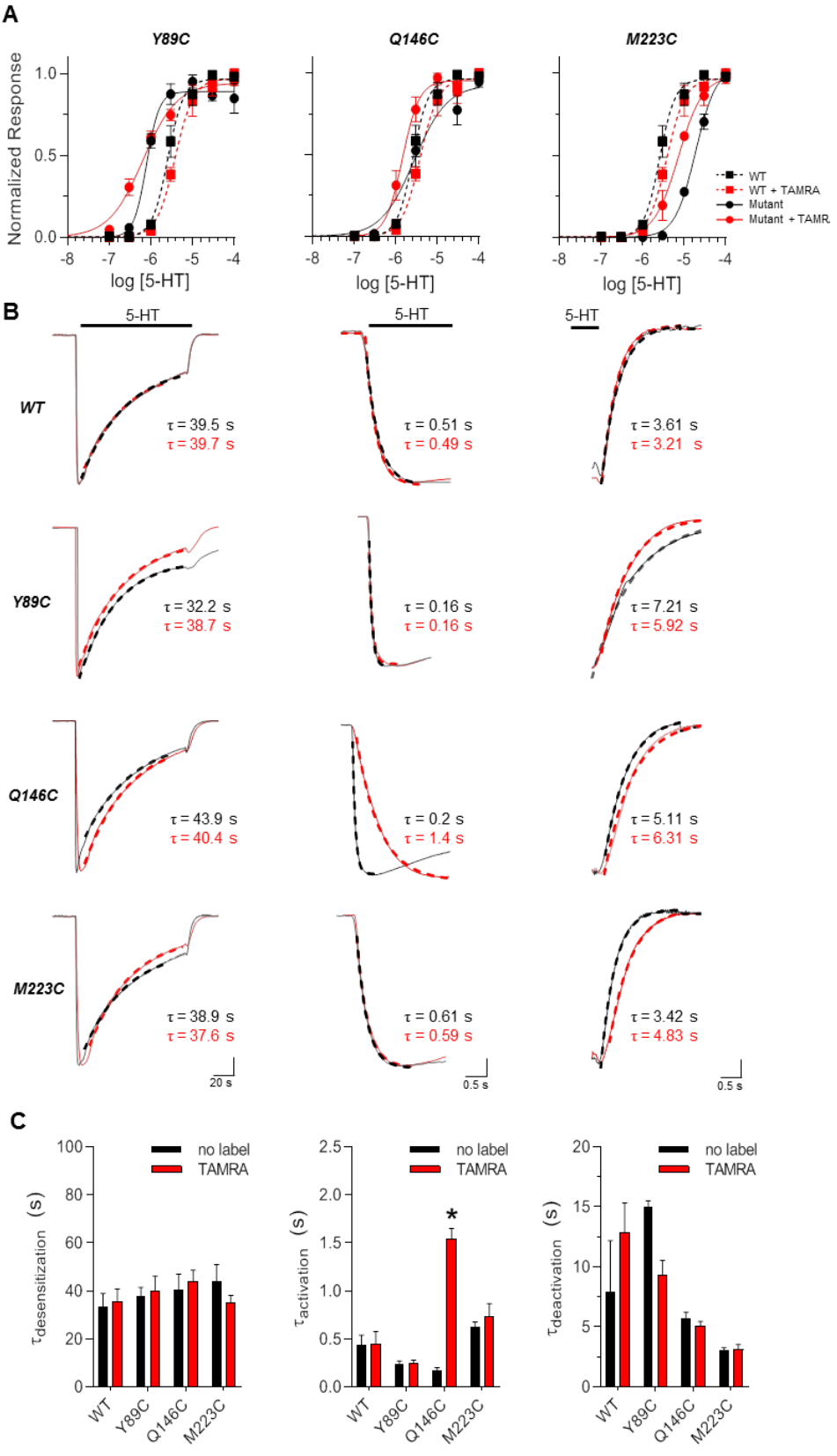

Molecular Pharmacology Fast Forward. Published on October 3, 2019 as DOI: 10.1124/mol.119.116657
This article has not been copyedited and formatted. The final version may differ from this version.

Figure 3

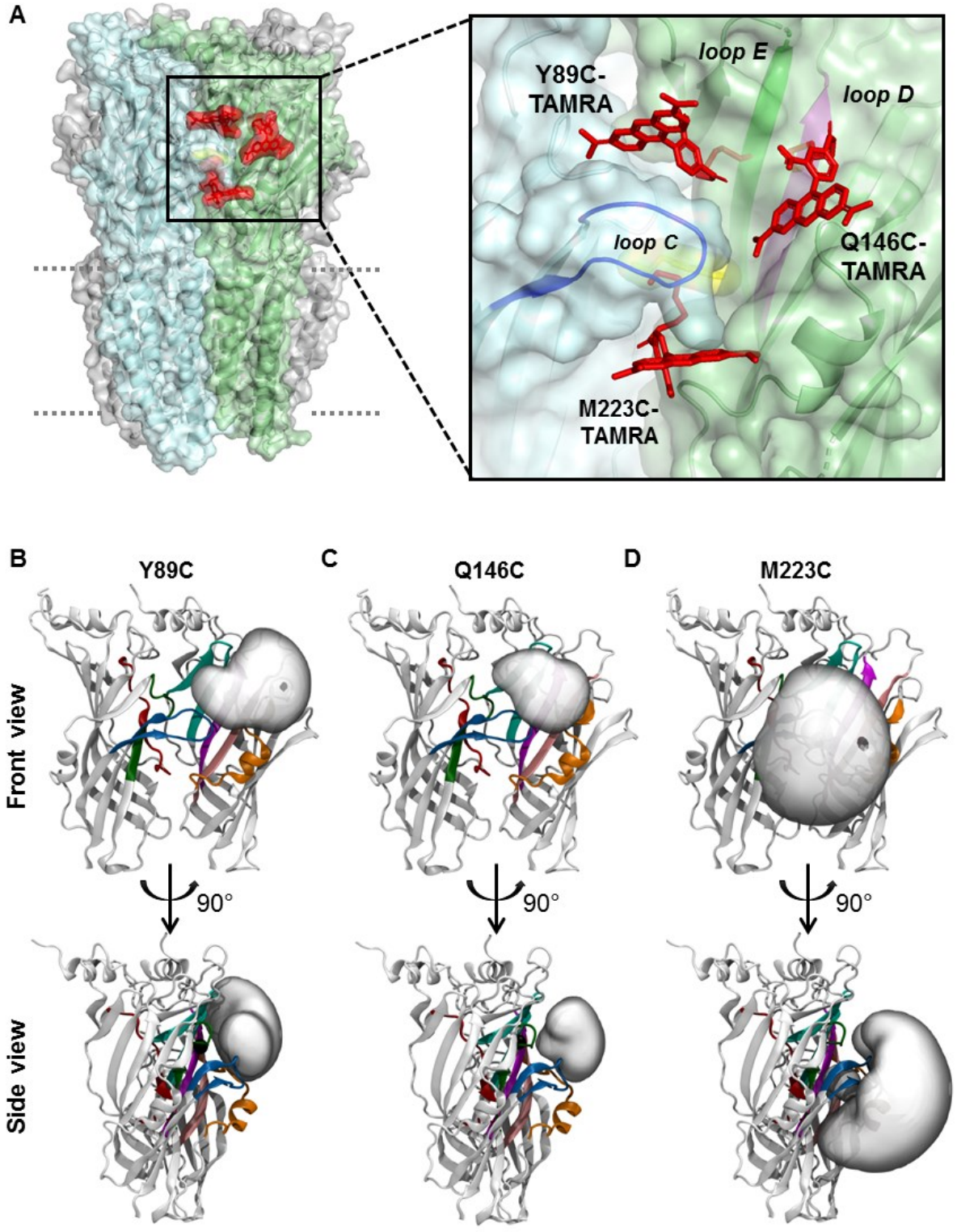

Molecular Pharmacology Fast Forward. Published on October 3, 2019 as DOI: 10.1124/mol.119.116657
This article has not been copyedited and formatted. The final version may differ from this version.

Figure 4

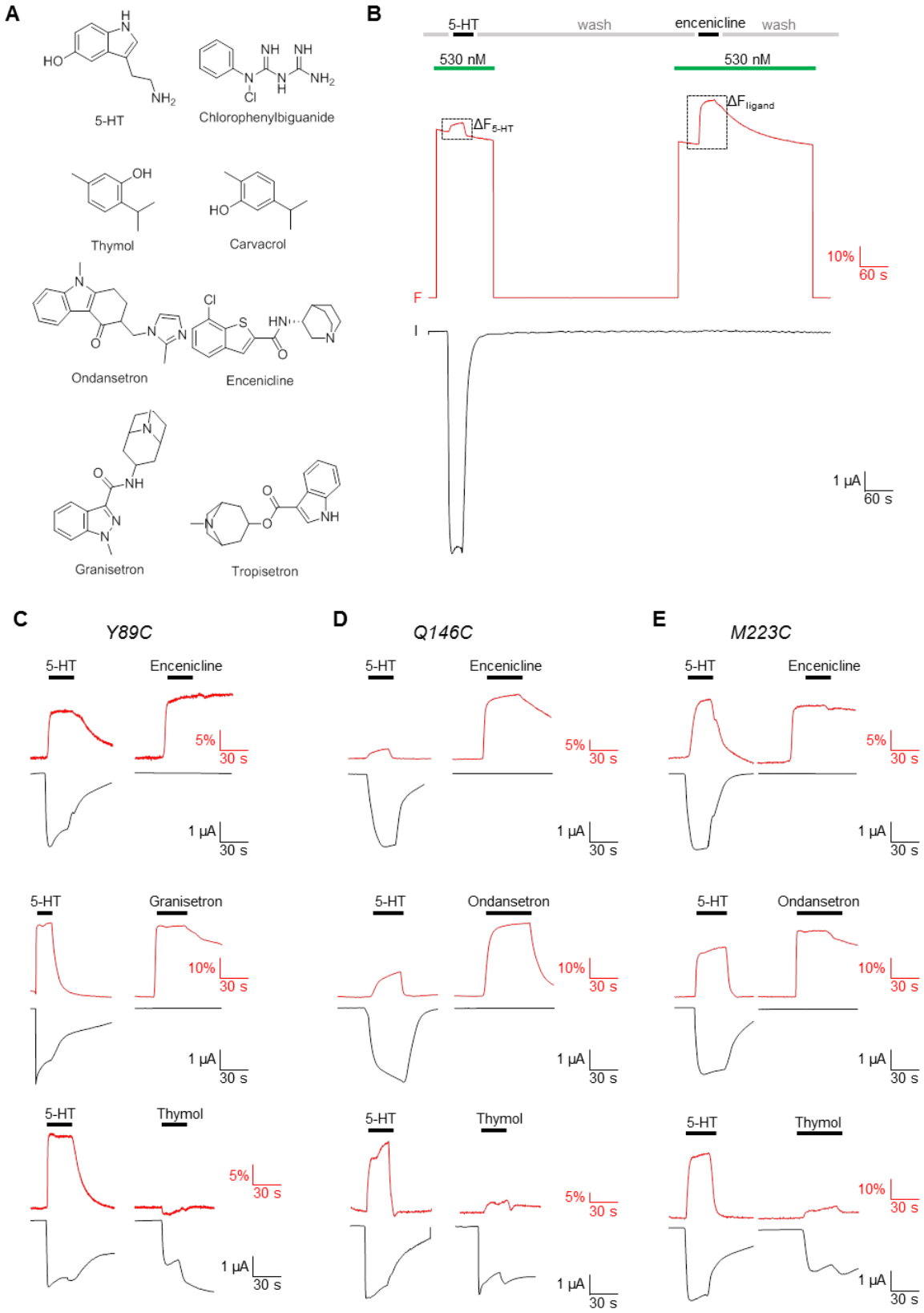

Molecular Pharmacology Fast Forward. Published on October 3, 2019 as DOI: 10.1124/mol.119.116657
This article has not been copyedited and formatted. The final version may differ from this version.

Figure 5

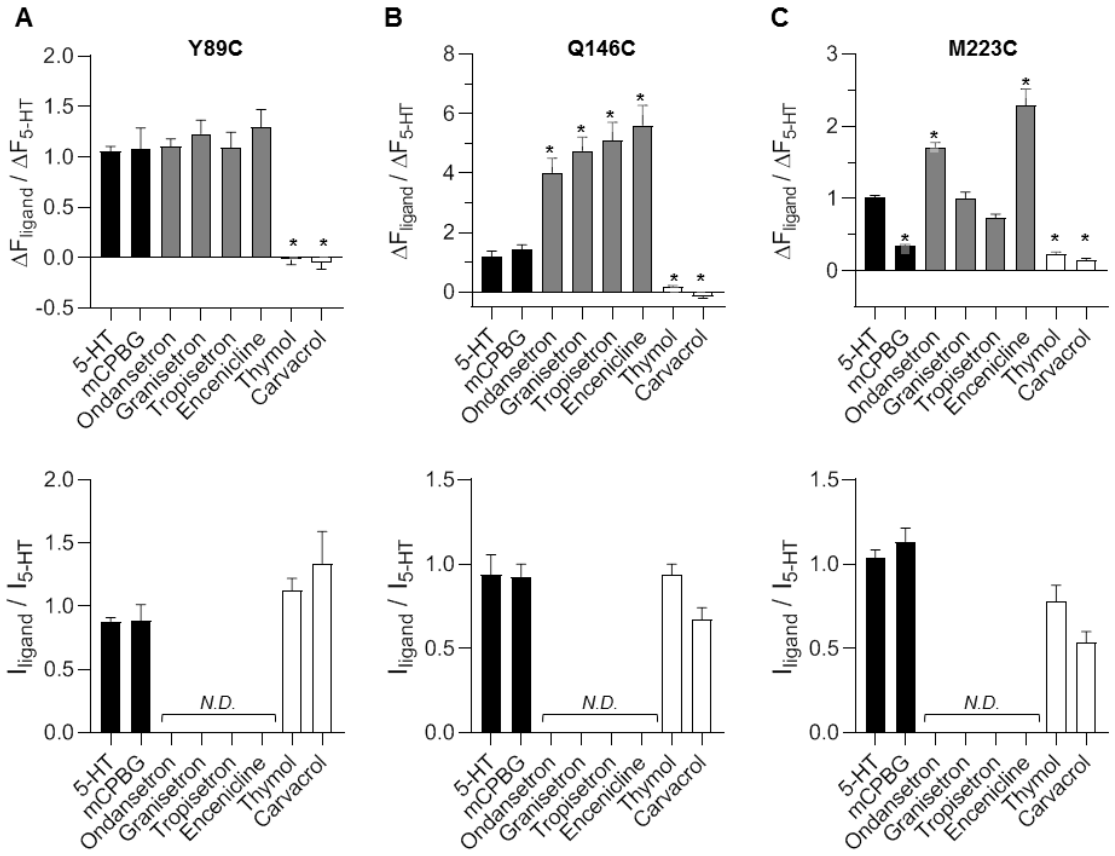

Molecular Pharmacology Fast Forward. Published on October 3, 2019 as DOI: 10.1124/mol.119.116657
This article has not been copyedited and formatted. The final version may differ from this version.

Figure 6

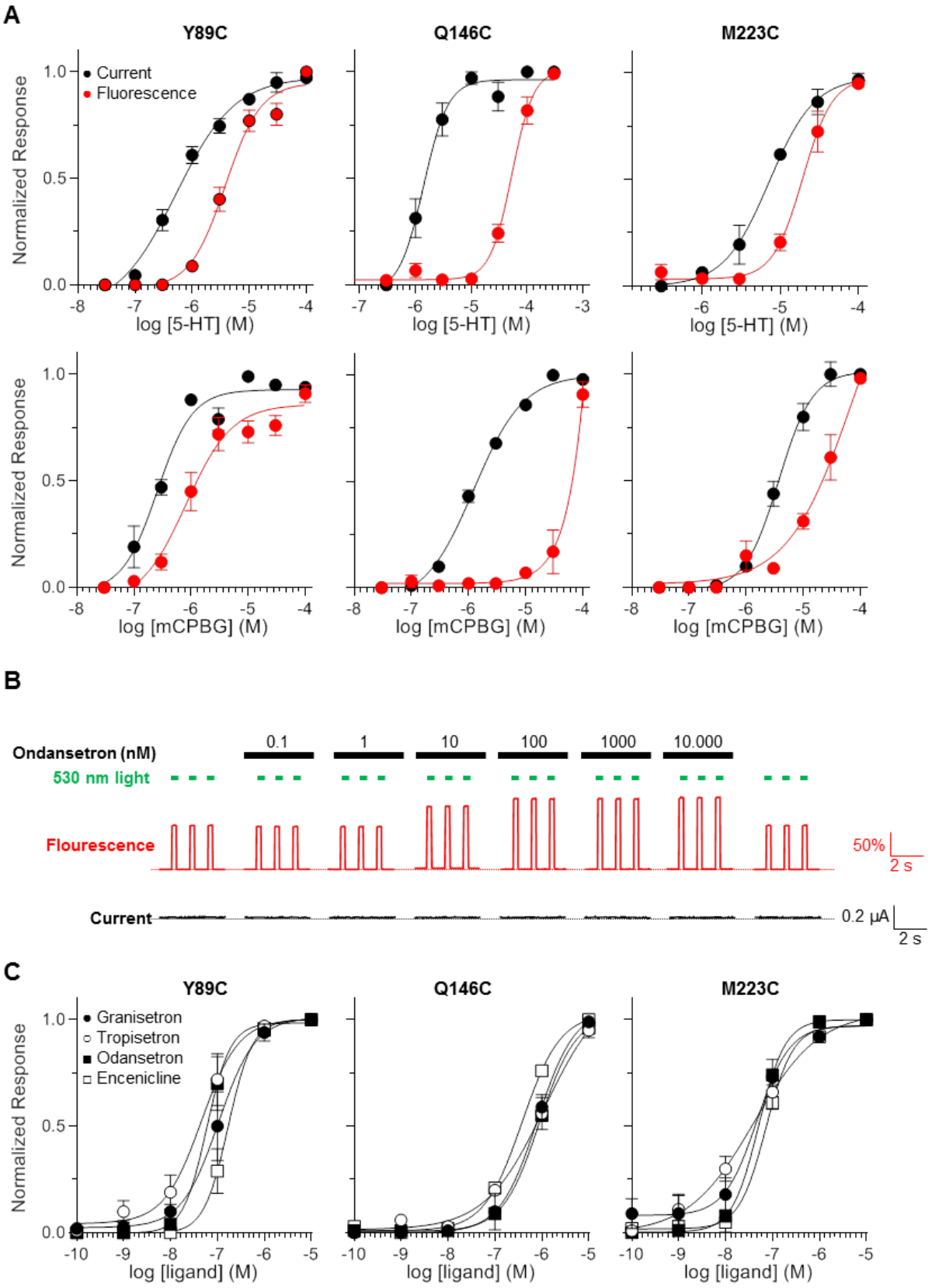

Supporting Information for

Conformational Changes in the 5-HT_{3A} Receptor Extracellular Domain Measured by Voltage Clamp Fluorometry

Lachlan Munro[1], Lucy Kate Ladefoged[2], Signe Andersen[1], Birgit Schiøtt[2, 3], Anders S. Kristensen[1]

[1]Department of Drug Design and Pharmacology, University of Copenhagen, Universitetsparken 2, DK-2100 Copenhagen, Denmark

[2] Department of Chemistry, Aarhus University, Langelandsgade 140, DK-8000 Aarhus, Denmark

[3]Interdisciplinary Nanoscience Center (iNANO), Aarhus University, Langelandsgade 140, DK-8000 Aarhus, Denmark

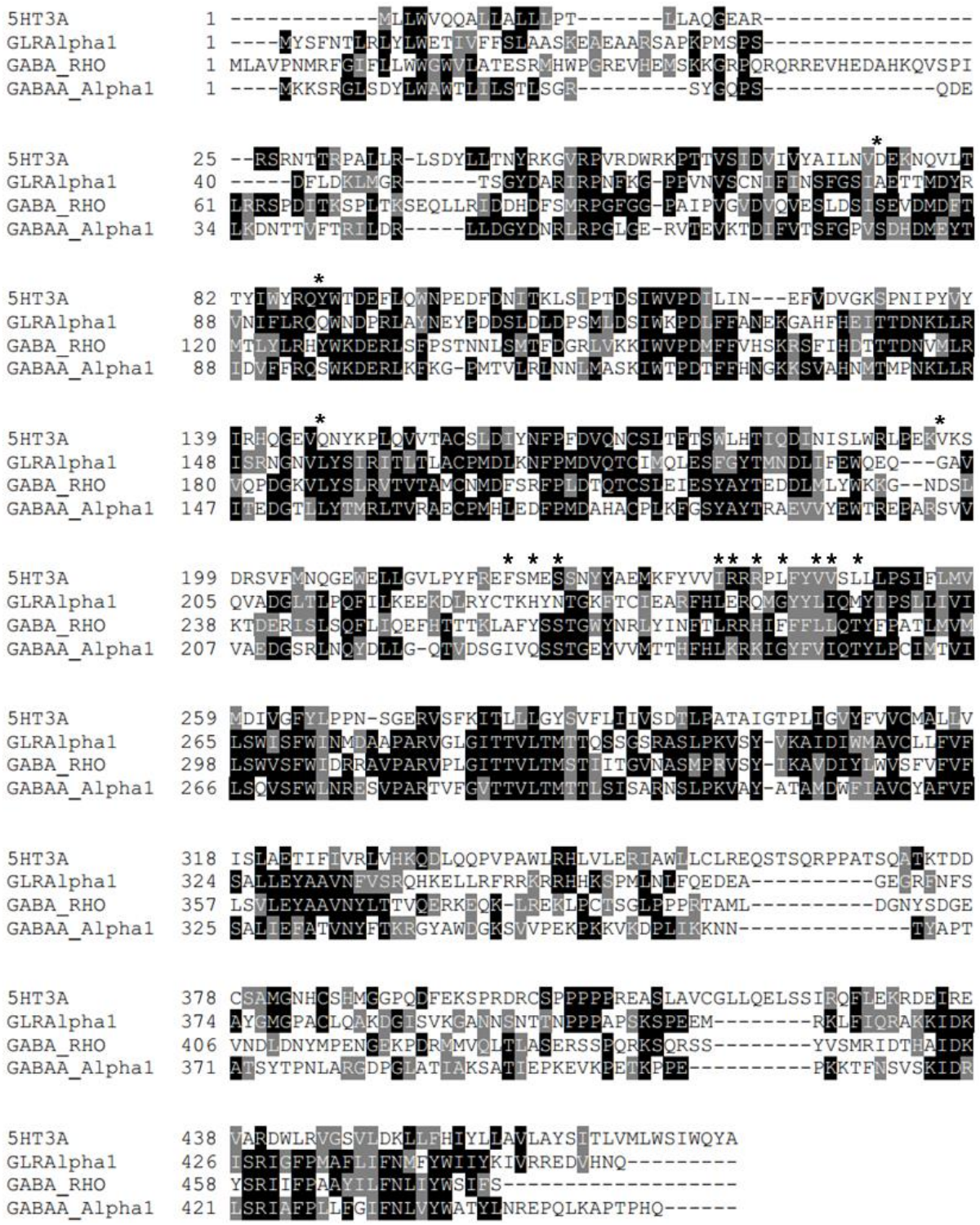

Figure S1. **Alignment of amino acid sequences for the 5-HT$_{3A}$ receptor subunit and pLGIC receptor subunits for which previous work has identified VCF reporter positions.** Sequences correspond to the human 5-HT$_{3A}$ subunit (5HT3A; UniProtKB accession code P46098) used in the present study, the human glycine receptor α1 subunit (GLRAlpha1; UniProtKB accession code P23415) used in Pless *et al*. (2009*a*,*b*), human GABA$_A$ receptor ρ subunit (GABA_RHO; UniProtKB accession code P24046) used in Chang *et al.* (2002) and Zhang *et al.* (2009), and the rat GABA$_A$ receptor α1 subunit (GABAA_Alpha1; UniProtKB accession code P62813) used in Muroi *et al.* (2006). *; indicates positions tested in the present study as potential VCF reporter positions.

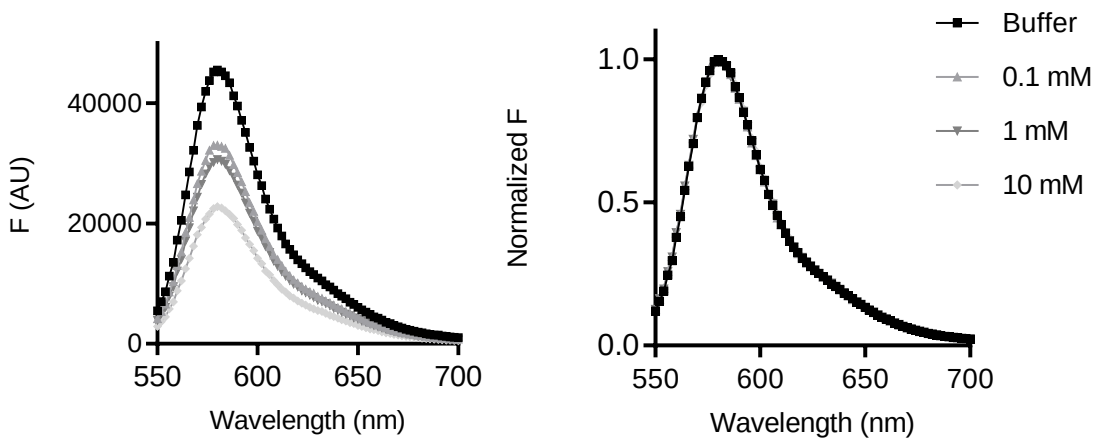

Figure S2. Effect of 5-HT on MTS-TAMRA fluorescence in solution. Emission spectra of MTS-TAMRA (20 µM) dissolved in Frog's ringer solution in absence and presence of 5-HT (*left*). Peak fluorescence is quenched by increasing concentrations of 5-HT as indicated. Normalized emission spectra (*right*; calculated relative to the peak of the MTS-TAMRA emission at 580 nm) show that peak emission wavelength is unchanged by 5-HT. MTS-TAMRA was prepared in phosphate buffered saline (PBS, in mM: 137 NaCl, 2.7 KCl, 10 Na2HPO4, 1.8 KH_2PO_4, pH 7.4) at a concentration of 10 µM in the absence and precence of increasing concentrations of 5-HT concentration (0.1, 1 and 10 mM). For each preparation, 20 µL was distributed into wells in flat bottom 96-well plate. Fluorescence emission spectra were obtained using excitation at 530 nm in a Safire2™ double-monochromator 96-well fluorimeter (Tecan, Grödig bei Salzburg, Austria) (*Supplementary methods*).

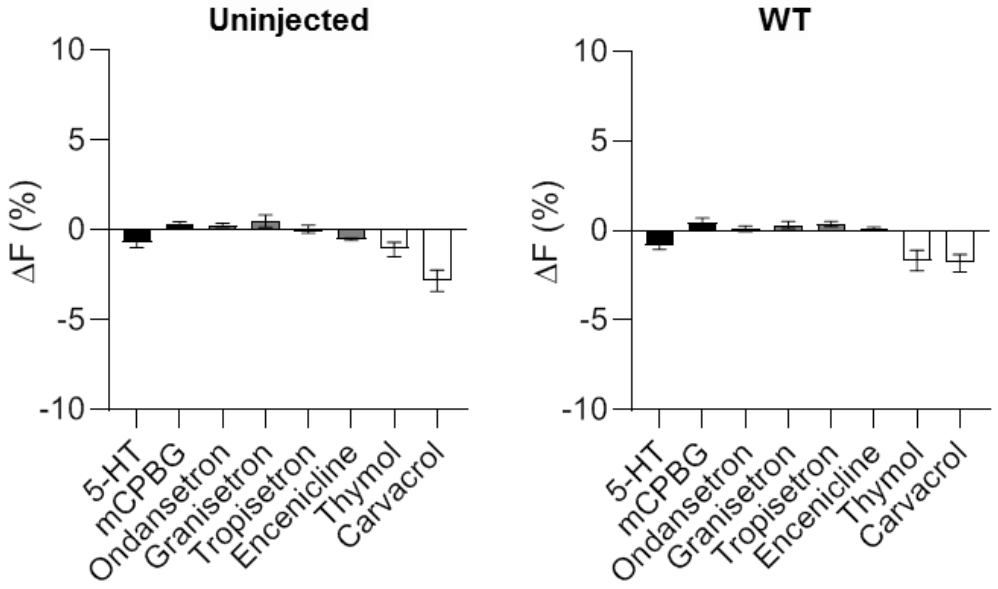

Figure S3. Effect of application of various ligands on conjugated TAMRA fluorescence at uninjected and WT 5-HT$_{3A}$ expressing oocytes. Shown are the mean of the measured ΔF (%) in response to application of highest concentration of ligands that were used in the present study at oocytes uninjected (*left*) oocytes or expressing WT h5-HT$_{3A}$ receptors (*right*). Error bars represent the S.D. of 3 or more individual oocytes.